Hindawi
Geofluids
Volume 2019, Article ID 2918673, 24 pages
https://doi.org/10.1155/2019/2918673

*Research Article*

# Fault Core Thickness: Insights from Siliciclastic and Carbonate Rocks

**A. Torabi**,[1] **M. U. Johannessen**,[1,2] **and T. S. S. Ellingsen**[1,2]

[1]*Norwegian Research Centre (NORCE), Nygaardsgaten 112, 5008 Bergen, Norway*
[2]*Department of Earth Science, University of Bergen, P.O. Box 7800, 5020 Bergen, Norway*

Correspondence should be addressed to A. Torabi; anita.torabi@norceresearch.no

Received 30 October 2018; Revised 6 February 2019; Accepted 17 March 2019; Published 2 June 2019

Academic Editor: Fabien Magri



Fault core accommodates intense deformation in the form of slip surfaces and fault rocks such as fault gouge, cataclasite, breccia, lenses, shale smear, and diagenetic features. The complexity and variation in fault core geometry and thickness affect fluid flow both along and across the fault. In this study, we have investigated a total of 99 faults in siliciclastic and carbonate rocks. This has resulted in two large datasets that include 871 fault core thickness measurements ($T$) in siliciclastic rocks and 693 measurements in carbonates, conducted at regular intervals along fault elevations (fault height) on the outcrop or photos of the outcrop. Many of these measurements have been analyzed with respect to fault displacement measurements ($D$) in order to study the relationship between displacement and fault core thickness and to further uncover the fault growth process. We found that the fault type and geometry, displacement, type of fault rocks, lithology, and competency contrasts between faulted layers lead to significant variations in the fault core internal structure and thickness. Analysis of average values of fault core thickness-displacement data of this study and of previously published studies shows that the core thickness-displacement relationship follows an overall power law, in which its exponent and intercept change depending on the lithology of the faulted rocks. In general, small faults in carbonate and siliciclastic rocks ($D \leq 5$ m) show comparable $T/D$ ratios, with a slightly higher ratio in carbonate rocks. The outcomes of this study contribute to the understanding of the fault core internal structure and variation in fault core thickness as a result of the interplay between fault displacement and host rock in different lithologies. These outcomes have significant implication for characterizing the sealing and conductivity potential of faulted rocks, which is relevant to different applications such as petroleum exploration and development of existing fields, hydrogeology, geothermal energy storage and extraction, and $CO_2$ sequestration.

## 1. Introduction

Faults play a significant role in controlling fluid flow and fluid-rock interactions in the shallow part of the crust. Faults can act as both barriers and conduits for fluid flow (e.g., [1–5]). This has resulted in significant studies on fault zone architecture, fault geometric attribute scaling laws, and sealing properties of faults ([6–11], among others). The deformed rocks within a fault zone can be divided into low-strain and high-strain zones commonly referred to as the damage zone and fault core, respectively [2, 3, 11]. Fault core accommodates fault rocks and most of the displacement and deformation [1, 4, 6, 12, 13]. Fault core is surrounded by the damage zone, which commonly includes minor faults, fractures, deformation bands, and fault-related folds [13–15]. The fault core is usually enveloped between the main slip surfaces and may include small slip surfaces and fault rocks such as fault gouge, breccia, clasts (rock fragments) and lenses of host rock, shale smear, and diagenetic features (Figures 1 and 2). Fault breccia and gouge are formed by progressive shearing and crushing of host rocks during the linkage of shear fractures in the relay zones and fault bends (e.g., [3, 16]). Thoroughgoing slip surfaces of the fault can be related to a thin veneer of gouge, originated from fine crushed host rock or shale [16].

Fault geometric attributes include fault displacement, length, damage zone width, and fault core thickness [2, 13]. Among fault attributes, the fault core thickness is the most

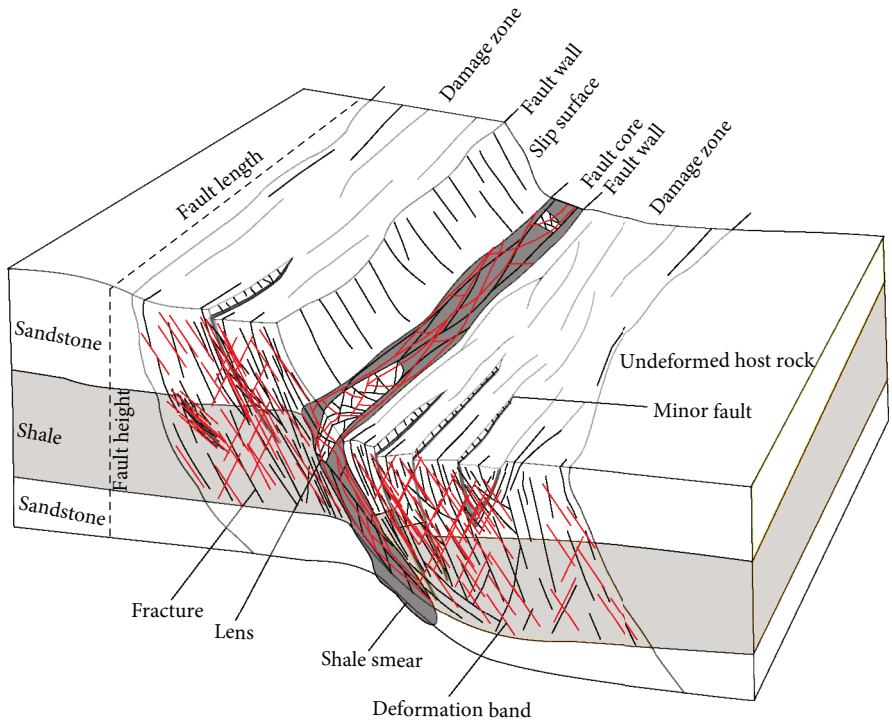


Figure 1: An illustration of a normal fault and its geometric attributes. Boundaries of fault core and damage zone and their internal structures are presented.

uncertain attribute. This attribute is considered as the key element when predicting the sealing or transmissivity potential of a fault zone. Due to the accommodation of displacement and intense deformation [4], the fault core affects the petrophysical properties of its enveloped rocks and hence influences the fluid flow in the rocks. Knowledge of fault core dimension and properties is needed for better reservoir/aquifer characterization and for developing more realistic fluid flow models. These would be beneficial for petroleum exploration and development of existing fields. Furthermore, this knowledge would be useful for other applications, such as hydrogeology and geothermal energy storage and extraction, and for evaluation of the best candidate reservoir to safely store waste and $CO_2$ in the subsurface ([17]; Besnse et al., 2013; [18–20]).

The thickness of a fault core can considerably vary from a millimeter-thick core with one simple slip surface to a zone containing several slip surfaces and intensely deformed rocks, up to several meters thick. On seismic data, the fault core thickness and its geometry are hard or impossible to capture, due to seismic resolution (e.g., [21]). Thus, the fault core structure and geometry are usually captured through accessible 2D sections of faults in the outcrops. There are uncertainties in the fault core data that could be related to (i) inconsistent definitions among geoscientists, (ii) complexity of the fault core, and (iii) rapid variation in fault core thickness over short distances along the fault. This rapid variation in core thickness was reported along the fault height, at fault jogs, and where variation in lithology occurs along the fault [13, 22, 23]. There is no standard definition of the fault core and its boundaries, and the core thickness measurements have often been subjective [3, 9, 13]. In the literature, there is inconsistency in the use of terminology describing the fault core (e.g., [2, 3, 9, 11, 16, 24–26]). This uncertainty in definition and terminology of the fault core and its boundaries makes constraining the dimensions of this attribute challenging. This has significant implications for characterizing the sealing potential and transmissivity of faulted rocks. This is particularly important in carbonate reservoirs [27] since there are less studies on fault seal analysis of such reservoirs than siliciclastic reservoirs. Therefore, in this study, we aim to characterize the fault core and constrain its boundaries by identifying the fault rocks enveloped within the fault core in both siliciclastic and carbonate rocks.

Researchers studied the relation between displacement and fault core thickness (e.g., [6, 16, 26, 28]) in order to predict the uncertain fault core thickness and understand the growth process of faults. A power law relationship ($T = aD^n$) between the fault core thickness ($T$) and fault displacement ($D$) was reported by many authors [7, 9, 16, 25, 29, 30]. Previous authors identified the variation of fault core thickness along the fault strike and dip (e.g., [9]) and the effect of juxtaposition of layers of different properties/competencies (such as shale and sandstone) on the fault core thickness and therefore on its scaling relation with displacement (e.g., [30]). Kolyukhin and Torabi [31] used a statistical approach called the Bayesian information criterion (BIC) on the compiled data from the literature [13] and suggested that the fault core thickness-displacement power law relationship could vary with the fault type, lithology, and size of the fault.

We have conducted an extensive study on the fault core in both siliciclastic and carbonate rocks to investigate the

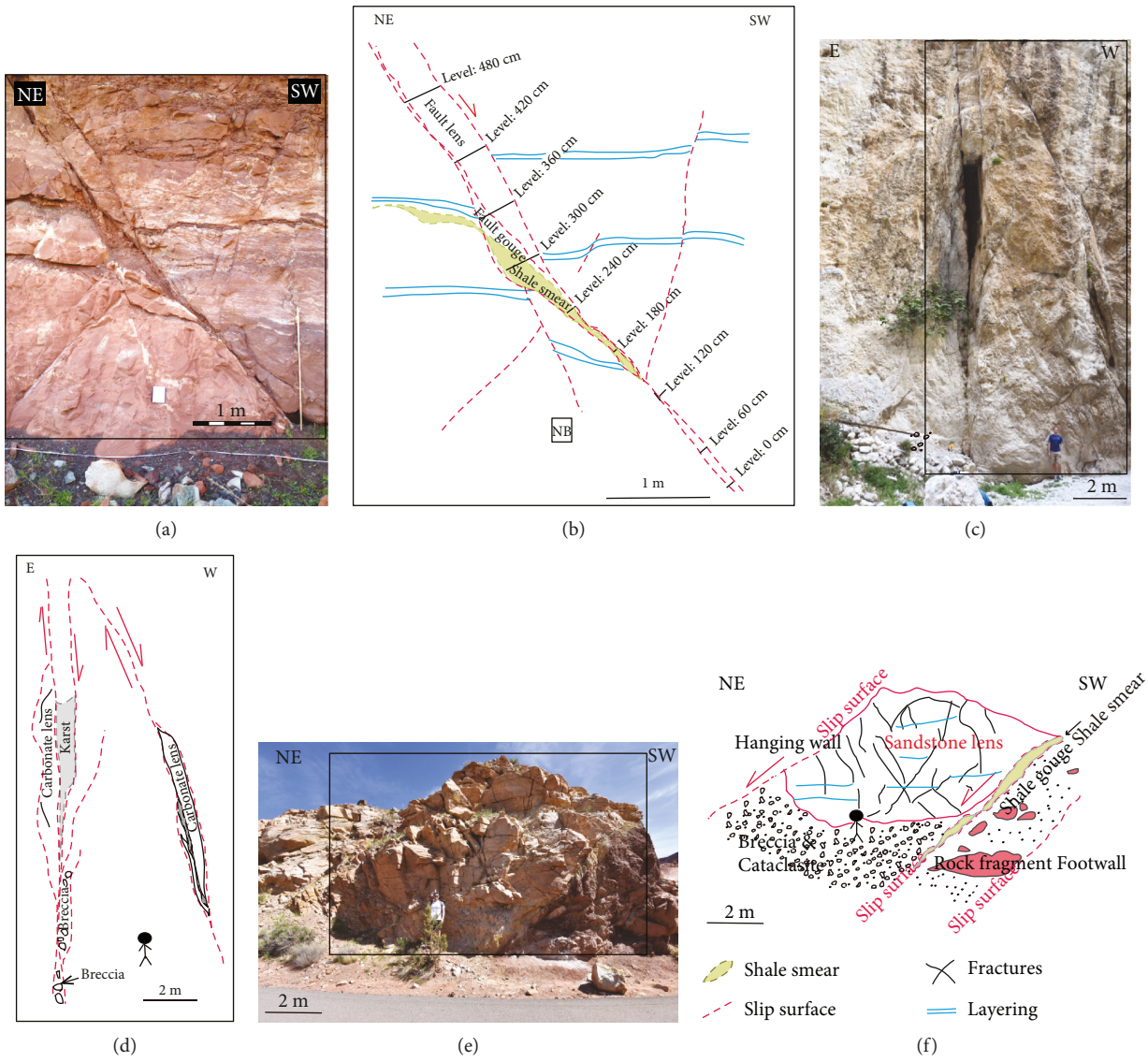


FIGURE 2: (a, b) Pictures of the outcrop with its sketch illustrating the method for measuring fault core thickness at the outcrop and on photos. The data collection started at the fault position on the scanline and fault core thickness (black lines) was measured perpendicular to fault walls at regular increments (levels) along fault height, in this case, every 60 cm. After Johannessen [70]. Note that the upper part of the figure might be considered as two faults with separate fault cores or splays of the same fault cropping out a lens. NB in (b) stands for notebook. (c–f) Examples of fault rocks (pictures and sketches) in the studied fault cores for carbonate rocks of Maiella and siliciclastic rocks of Utah. Multiple slip surfaces, carbonate lenses, karst (not included in the measurements), and breccia are among the structures found in the fault core of carbonate rocks in the strike-slip fault in Maiella in (c) and (d). Note the presence of several slip surfaces and shaley gouge with rock fragments as well as breccia and cataclasite in a normal fault (R-191) in (e) and (f).

effect of the lithology on the fault core thickness and displacement. Our siliciclastic dataset was obtained from faults in Utah, USA, while the carbonate dataset was acquired from faults in the Maiella Mountain in Italy. Furthermore, we have studied different types of faults (normal, strike-slip, and reverse) in carbonate rocks, while only normal faults were studied in siliciclastic rocks. A specific aspect of this study is capturing the variation of fault core thickness along fault exposures by measuring the thickness at regular intervals along the fault height in vertical sections (Figure 2(a)). We provide new datasets of fault core thickness and displacement, which are compared with the previously published data in order to study the relationship between these fault geometric attributes and improve the prediction of fault core thickness when dealing with faults in rocks of different lithologies.

## 2. Methods

The database analyzed in this study consists of 99 faults, including 94 small faults ($D < 10$ m) and 5 large faults with a displacement of up to ~1 km. This database includes a total of 1564 fault core thickness measurements, with 871 measurements from siliciclastic rocks (Utah, USA) and 693 measurements from carbonates rocks (Maiella Mountain,

Italy). At the studied localities, a 50 m measuring tape was laid out at the base of the outcrop to define an area of interest along the fault zone in the outcrop. The scanline was used for positioning different faults at the outcrop. The fault core thickness was primarily measured on isolated fault segments, but examples of overlapping and linked fault segments are also present in the datasets. The fault core boundaries were constrained by the volume of fault rocks located between the thoroughgoing synthetic slip surfaces, which separated the fault walls (hanging wall and footwall). The thickness was measured perpendicular to these defined boundaries (Figure 2(a)). Fault rocks including fault gouge, breccia, rock fragments and lenses of host rock (which can be excluded from the measurements), shale smear, and diagenetic features are identified by deformation and chemical alteration and cementation compared to the surrounding wall rocks (Figures 1 and 2). We define the fault core thickness as the total thickness of fault rocks incorporated in the fault core and by identifying the thickness of permeable parts of the fault core such as lenses separately. This would allow excluding the thickness of lenses from the total fault core thickness when predicting the scaling and fluid flow properties of fault rocks in Results. We consider shale smear as part of the fault core even though that the bounding slip surfaces are not breached (Figures 1 and 2). Where a fault was observed along the scanline, the position of the fault was recorded and fault core thickness was measured along the fault height at different elevations (levels) every 60 or 30 cm, if great variation was observed along the fault core (Figure 2(a)). For each studied outcrop, we also recorded the fault type, fault orientation, fault displacement (if possible), and description of fault rocks situated in the core.

Since many of the outcrops were steep exposures and not totally accessible, the data gathering in the field was generally limited to the lowermost 3-4 m. Photos of the studied faults were taken at the outcrops and further used to verify and collect more core thickness and displacement measurements for the areas not accessible in the field. The measurements were completed at intervals similar to outcrop measurements or at points where displacement was measurable. The photo measurements from the lower levels of outcrops were compared and correlated with the corresponding field measurements to verify the accuracy of the measurements. The optimal measurements are obtained from photos parallel to the strike of the fault, which are measured close to the center of the photo [32]. However, as this could not be possible for some of the measurements, some distortion of photos is expected, which can potentially affect the measurements. For the Utah dataset, a total of 145 photo measurements could be compared to the field measurements and a linear relationship was found between the photo and field measurements of fault core thickness:

$$y = 1.02x + 0.93, \quad R^2 = 0.96. \tag{1}$$

While for the Maiella dataset, 178 measurements could be compared and the following linear relation was obtained between the fault core thicknesses measured on the photos and outcrop:

$$y = 0.88x + 1.08, \quad R^2 = 0.94. \tag{2}$$

## 3. Results

*3.1. Faults in Siliciclastic Rocks.* The studied faults are located in siliciclastic rocks exposed in five outcrops in the southeastern part of Utah around the Moab Fault zone (outcrops 1-4) and in the Humbug Flats (outcrop 5) (Figure 3). In total, 871 measurements were conducted on fault cores in siliciclastic rocks. A description of the geological setting is presented in Appendix (Figure 15). The outcrops are shortly presented along with the results from outcrop measurements as follows:

*3.1.1. Outcrop 1.* The R-191 Canyon is located along the Moab Canyon, about 11 km northwest of the Moab Town. We conducted a 100 m scanline at the base of the outcrop at this locality, where two normal faults (F1 and F2) were measured. The damage zone of these faults is intensively fractured. The two normal faults (F1 and F2 in Figure 4) are part of the southern segment of the Moab Fault zone with accumulated displacement of up to almost 1 km [33]. F2 has accommodated most of the displacement ~950 m compared to F1, which has around 60 m displacement [25, 33]. F2 is oriented approximately parallel to the main trend of the Moab Fault, trending NW-SE with a dip of 44°NE, while F1 shows a different orientation (trending E-W with a dip of 24°N), and hence is considered as a splay of the main fault [25].

F1 is located at 45.5 m on the base scanline and displaces the Salt Wash Member of the Morrison Formation against the Moab Member sandstone lens (Figure 4(a)). F1 consists of two main slip surfaces, bounding a zone of grey shaley fault gouge derived from the Brushy Basin Member of the Morrison Formation with some sandstone fragments incorporated. At the upper part of the fault core (F1), the shaley fault gouge shows some color alteration due to iron oxide reduction in the gouge. The sandstone fragments in the fault core are likely to be from either the Salt Wash Member or the Moab Member [25].

The Moab Member lens is 12.7 m thick and is located between 53.0 and 65.7 m on the scanline, followed by F2, which includes two zones (zones A and B) separated by minor slip surfaces. F2 juxtaposes the Cutler Formation in the footwall versus the Moab Member lens in its hanging wall (Figures 4(a) and 4(b)). F2 encompasses four slip surfaces that accommodated fault rocks and shale smear in zones A and B [25]. Zone A consists of a beige to light-grey fault gouge and some scattered pods of cataclasite. The contact between zone A and the Moab Member lens is intensely fractured. Zone B consists of a thick zone of the reddish Cutler Formation that was smeared out and includes fragments of the pre-Wingate Sandstones.

In general, the fault core is thicker in F1 (1.6-2.4 m) in comparison to fault cores incorporated into the F2 zone

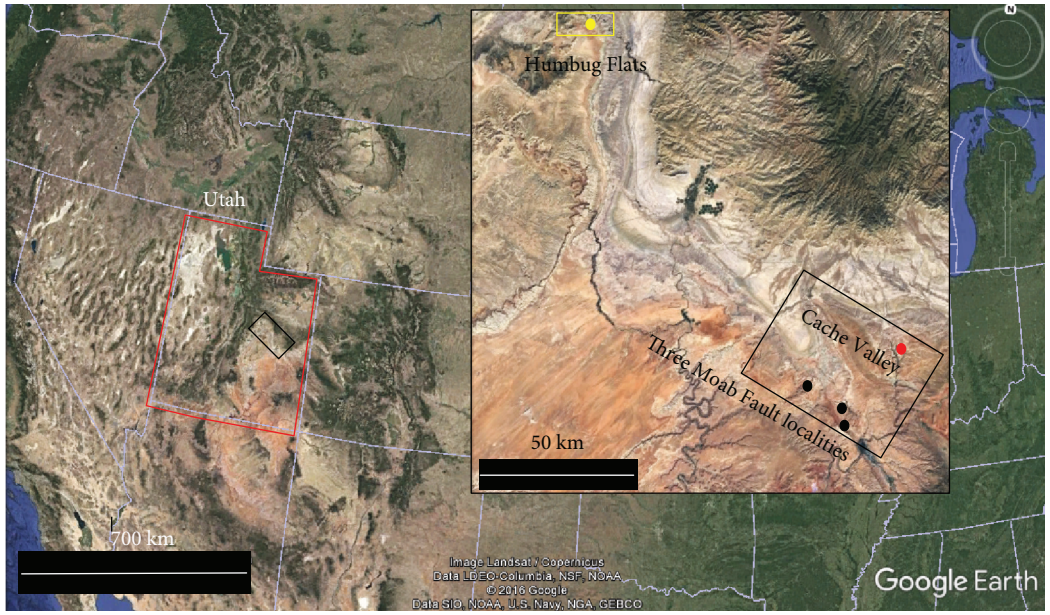


(a)


(b)

Figure 3: Google maps of the studied areas in Utah (USA) and Maiella (Italy). (a) Three localities studied around the Moab Fault and one in the Cache Valley are all in the Paradox Basin. The Humbug Flats outcrop is located in the San Rafael Swell. (b) The outcrops in Vallone di Santo Spirito were studied in the Maiella study area.

(0.2-2.30 m), which has a larger variation in thickness. When comparing zones A and B in F2, there is a substantial difference between the two, in which zone A is narrower than zone B, which includes a shale smear (Figures 4(b) and 4(c)).

*3.1.2. Outcrop 2.* This locality is located at ~25 km northwest of the Moab Town, where a segment of the Bartlett Fault exposed in the Hidden Canyon was studied. The displacement of this normal fault is estimated to be about 200 m [34]. This fault trends NW-SE with a dip of 63°NE. The fault displaces the Cedar Mountain Formation in the hanging wall against the Slick Rock and Moab Members of the Entrada Sandstone in the footwall. In the damage zones, fractures are dominant deformation features in the Cedar Mountain Formation. In the Entrada Sandstone, on the other hand, deformation bands are dominant with increasing frequency in the bleached layers of the Moab Member, which has high porosity (e.g., [35]). The fault rocks include a grey-beige fault gouge, which is covered with some debris in the middle part of the fault core, while the fault core boundaries are clear in the lower part of the outcrop. In addition, there are two lenses originating from the Moab Member

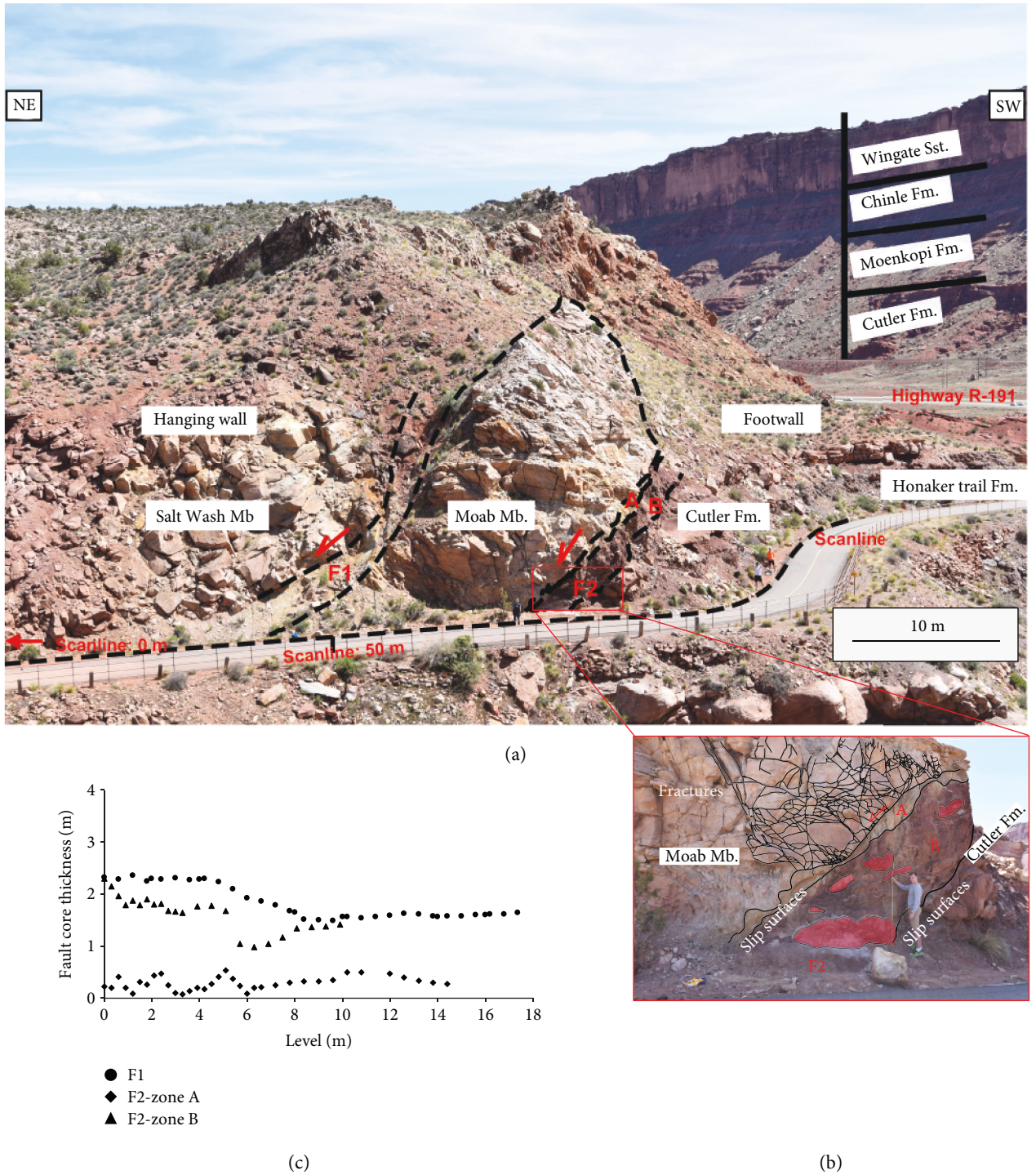


Figure 4: (a) Outcrop photo of the R-191 Canyon locality in Utah with a short description of stratigraphy and displaced formations. Note the locations of F1 and F2 (zones A and B) along the scanline at the base of the outcrop. (b) The inset is a closeup of the lower part of F2 zones, A and B. (c) Fault core thickness measured at different levels of the fault cores at this locality.

that are dragged into the fault core in this locality [14], (Figure 5(a)). The lower lens is thicker (3.28 – 9.17 m thick) and longer (46.5 m) than the upper lens (2.55 – 5.44 m thick), which is 14.5 m length. The upper lens is smaller than the lower lens. Cataclastic deformation bands, shear fractures, and slickenlines on fault surfaces are observed within these sandstone lenses. The lower lens is located in the fault core from level 0 m to level 46.5 m along the fault height, while the upper lens is from 54.5 m to 68 m from the base scanline (Figure 5). The fault core is wide even without including the thickness of lenses and involves several shaley fault gouge zones and slip surfaces, where each gouge zone can vary in thickness from 1 cm to ~10 m [25], (Figure 5(a)).

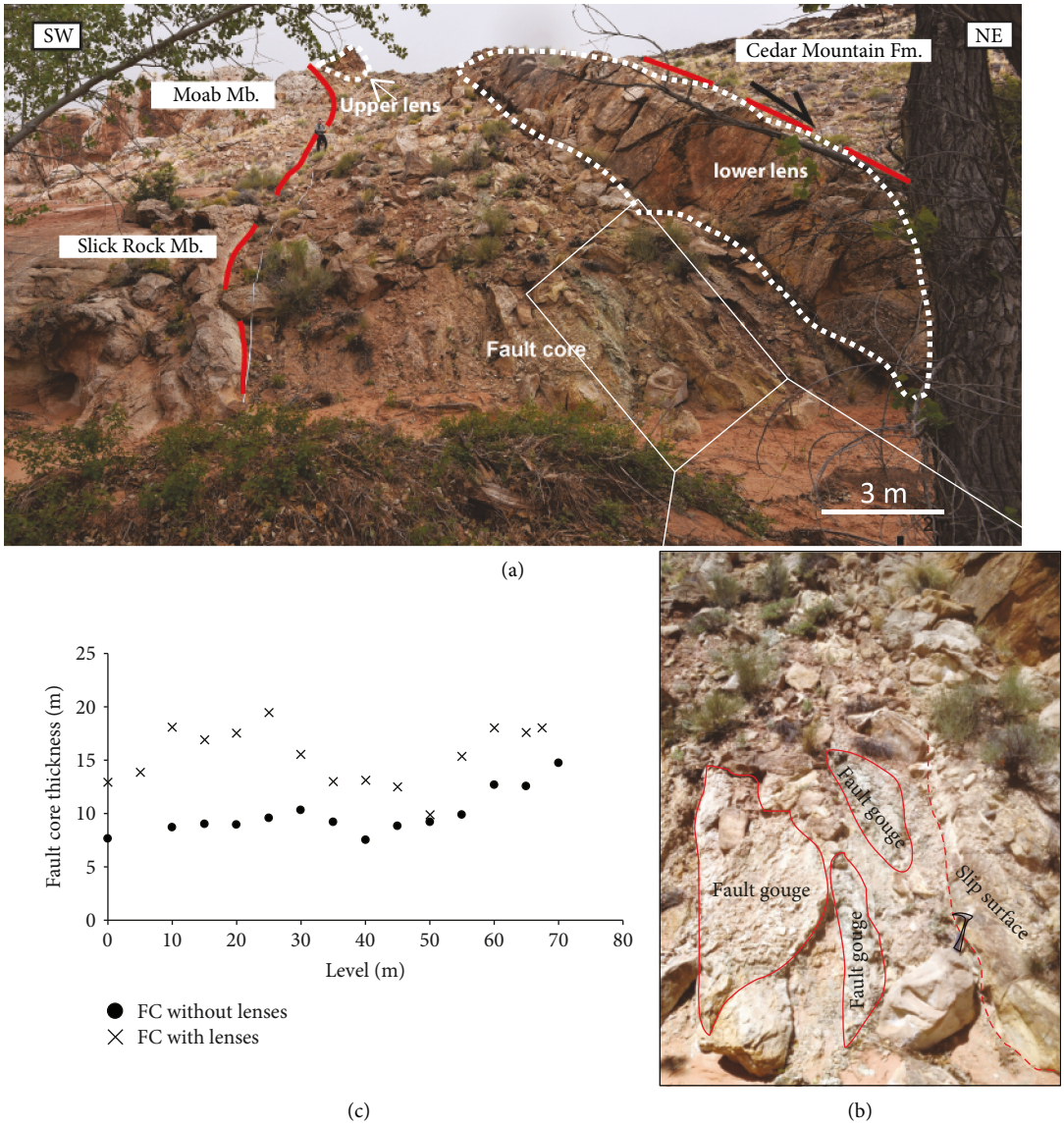


Figure 5: (a) Outcrop photo of the Bartlett Fault at the Hidden Canyon locality in Utah, which has displaced rocks of the Cedar Mountain Formation (hanging wall) against Slick Rock and Moab Members (footwall). (b) A closeup of the fault core showing several fault gouges and a major slip surface. (c) Fault core thickness (FC) measurements at the Hidden Canyon with and without including the lens thickness.

We have measured the thickness of the fault core first without including the lenses and then added the thickness of lenses at each level to the measured thicknesses (Figure 5(b)). The average fault core thickness increases from 10.91 m to ~16 m when including the thickness of sandstone lenses in the total fault core thickness.

*3.1.3. Outcrop 3.* This outcrop is located at the roadcut, across the Arches National Park (ANP) visitor center along Highway R-191. The small faults in this outcrop are part of the damage zone of the Moab Fault footwall, which forms the steep cliffs of the Moab Canyon (Figure 6(a)). Most of the faults are trending NW-SE parallel to the orientation of the Moab Fault. The Honaker Trail Formation, which is dominated by sandstones and shales, is exposed in this outcrop [36]. Fractures and small faults are dominant deformation features in this damage zone. In the fault cores, brown to greyish shale smear is observed in the faults displacing the lower shale unit of the Honaker Formation. Within some of the large faults that displace sandstone against shale layers, sandstone lenses are surrounded by shale smear. The larger faults, which juxtapose sandstone-sandstone units, include some cataclasite in the fault core. Since a total of 39 normal faults were measured along a 200 scanline in this outcrop, only average values of the fault core thickness and displacement measurements are presented in Figures 6(b) and 6(c). For displacement measurements, the marker layers were identified based on previous studies that classified the layers in this locality (e.g., [32]). The maximum displacement and fault core thickness measured for these minor faults are 9.5 m and 1.45 m, respectively. The minimum displacement and core thickness are 0.02 m and 0.01 m, respectively. The results (Figures 6(b) and 6(c)) show that fault core thickness ($T$) and displacement ($D$) are correlated and with increasing

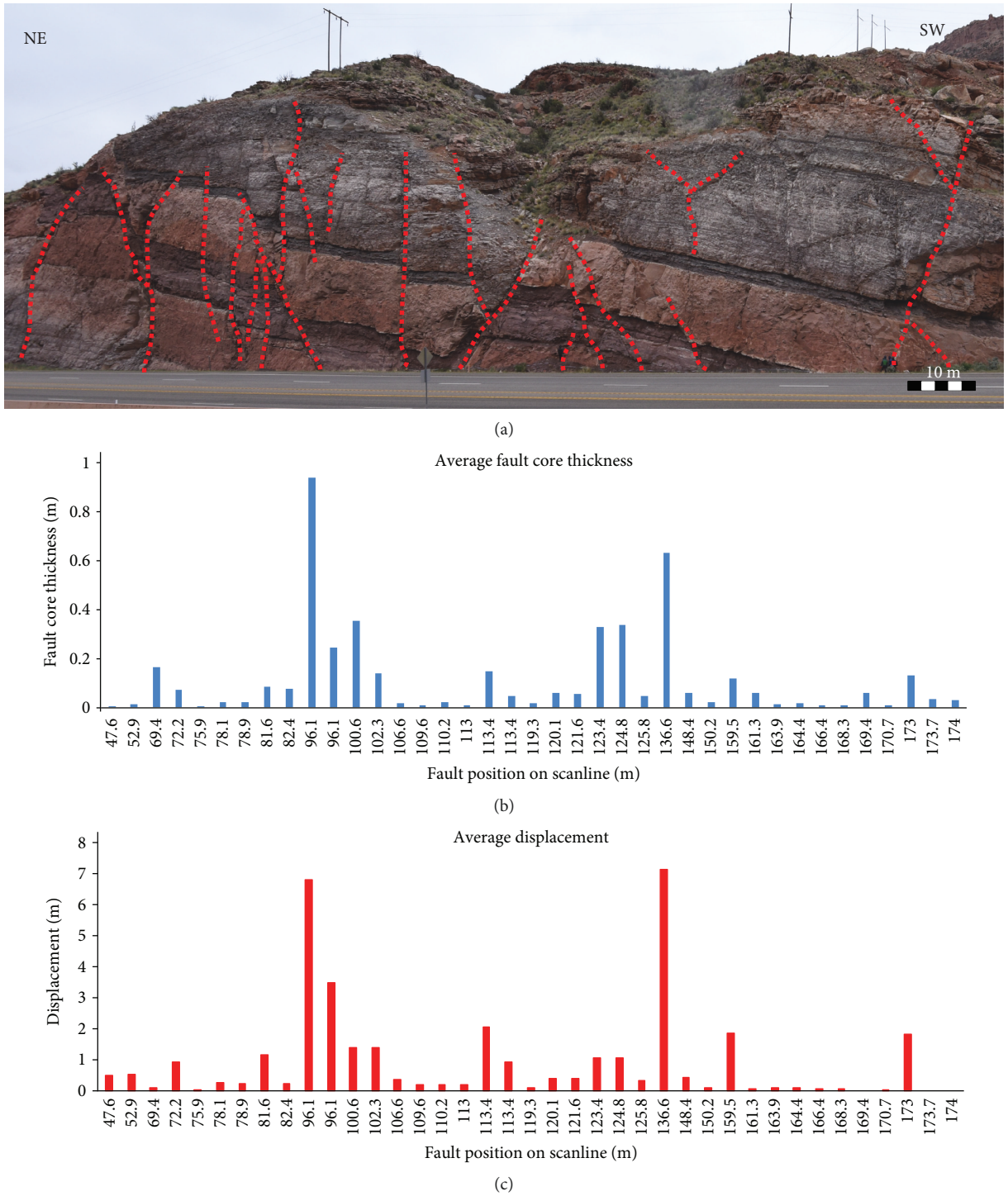


Figure 6: (a) Outcrop 3 (ANP), located across the Arches National Park visitor center. (b) The plot presents the average fault core thickness for each fault. (c) The plot presents the average displacement values for the corresponding faults.

displacement; the thickness of fault core increases with some exceptions that could be attributed to the lithological changes. A linear trend line ($T = 0.1D + 1.5$) fits to the displacement-fault core thickness data with the highest coefficient of determination ($R^2 = 0.80$) in comparison to other types of statistical relation that were examined by the authors. Note that in contrary to most of the studied localities, for each fault, several displacement and corresponding fault core thickness were measured, although the average values have been provided. Based on our observations, in faults displacing shaley layers, the fault core widens, regardless of the magnitude of displacement. In addition, contribution of fault lenses derived from the surrounding layers increases the core thickness in some of the faults.

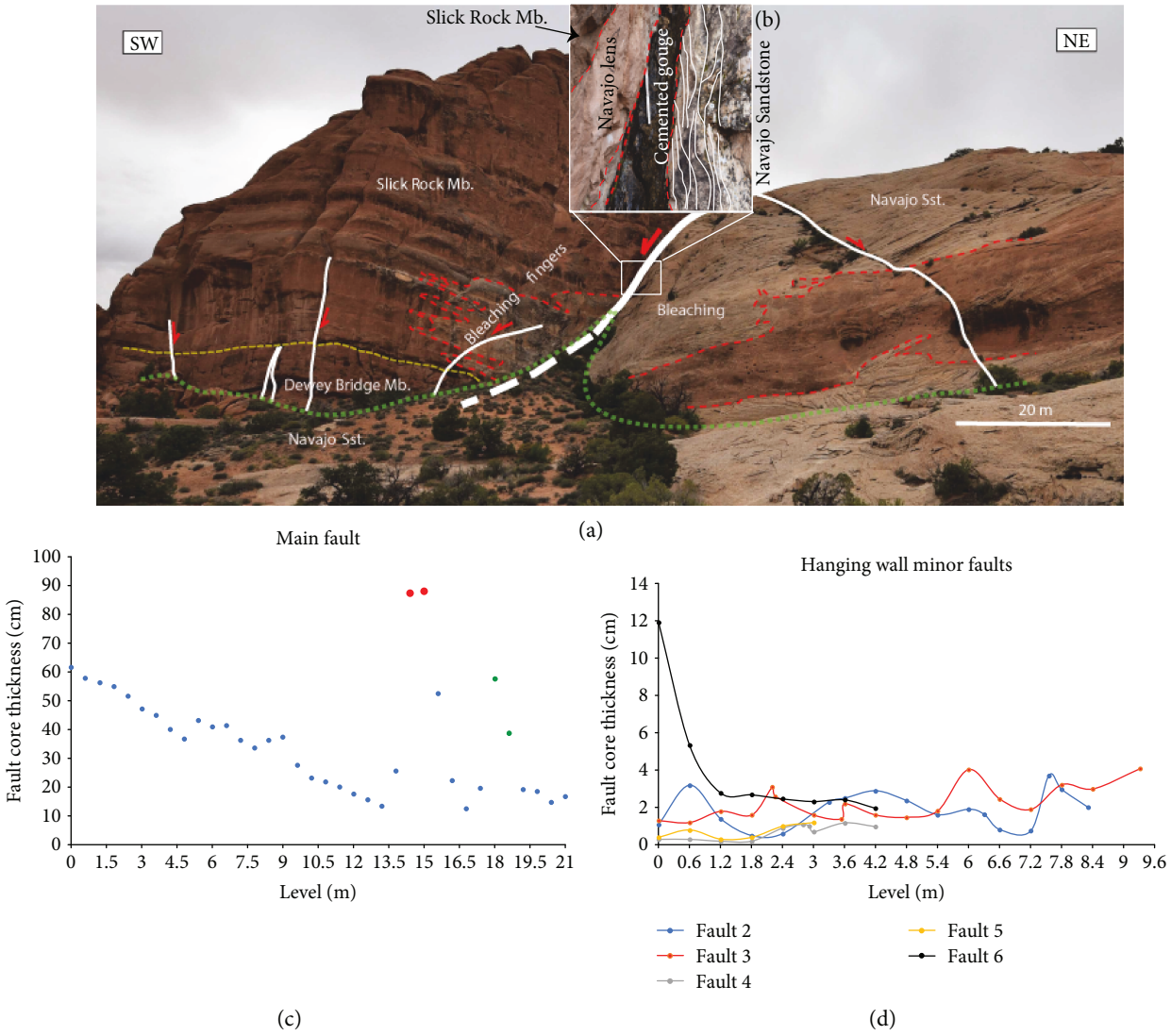


FIGURE 7: (a) A photo of the outcrop studied in the Cache Valley with stratigraphic boundaries and faults. The dashed green lines indicate the scanlines, and the yellow line indicates the boundary between the Slick Rock and Dewey Bridge Members. (b) A closeup of the fault core with its internal structures that include cemented gouge, cluster of deformation bands (white solid lines), and Navajo sandstone lens trapped between the slip surfaces. (c) The plot shows fault core thickness measurements on the main fault; colored symbols (in red and green) are related to thickness of two fault lenses. (d) The plot shows the fault core thickness measurements along the minor (smaller) faults in the hanging wall of the main fault.

*3.1.4. Outcrop 4.* Cache Valley is located along the eastern border of the Arches National Park. The main normal fault in this locality has an estimated displacement of around 30 m [37]. The main fault studied is subparallel to the axis of the Cache Valley salt-cored anticline, which is trending NW-SE and dips 71°SW [38, 39]. This fault displaces the Navajo Sandstone in the footwall against the Dewey Bridge and Slick Rock Members of the Entrada Formation in the hanging wall. Clusters of deformation bands are observed mostly in the footwall damage zone, where the porous Navajo Sandstone is located. Some parts of the Navajo Sandstone are bleached due to the removal of grain coating hematite [40]. Bleaching fingers are also observed in the hanging wall close to the main fault core, where the rocks of the Slick Rock Member are situated.

In addition to the main fault, six minor (smaller) faults in the hanging wall and one in the footwall were studied in detail (Figure 7(a)). These faults were measured along a 200 m scanline, which was laid out at the base of the outcrop. The fault rocks of the main fault consist of dark-black cemented gouge (mainly calcite with some iron oxide cement), host rock lenses trapped between slip surfaces and clusters of deformation bands (Figures 7(a) and 7(b)).

The main fault core thickness varies between 8 cm and 60 cm without considering the thickness of lenses. Including the thickness of lenses (up to 90 cm) can significantly increase the thickness of the fault core (Figure 7(c)). The minor normal faults show different ranges of fault core thickness and fault displacement. F6 has the thickest fault core among the minor faults in the hanging wall (Figure 7(d)). The minor fault

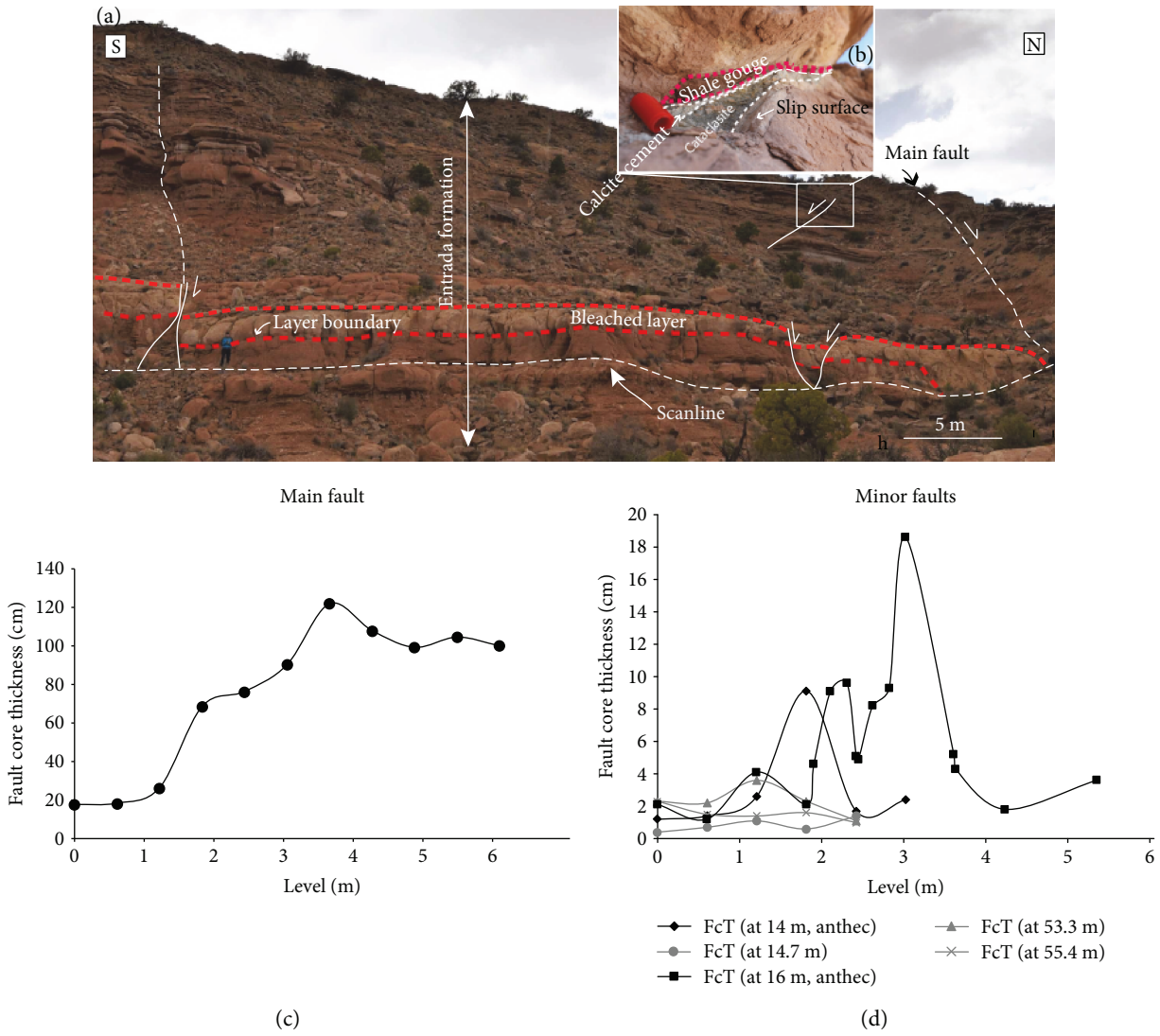


Figure 8: (a) Field locality in the Humbug Flats. Note the presence of main and minor faults that cross the 60 m scanline. (b) A closeup showing an example of the internal structure of faults in this locality. The fault core includes cataclasite, shale gouge, and calcite cement. (c, d) Fault core thickness measurements at different levels for the main and minor faults in this locality.

in the footwall intersects both bleached and unbleached intervals. Comparing the measured fault core thickness in the bleached and unbleached intervals, the fault core in the bleached interval is wider (8 – 37 cm thick) than the one in the unbleached interval (3 – 5 cm thick). This difference could be related to the higher porosity in the bleached intervals.

*3.1.5. Outcrop 5.* The Humbug Flats locality is on the northwestern part of the Colorado Plateau, close to the northern edge of the San Rafael Swell anticline. A main fault trending NW-SE with an approximate displacement of 40 m cuts through a part of the Entrada Sandstone, which is equal to the Dewey Bridge Member in southeast Utah and the Carmel Formation. A bleached layer is observed throughout the valley. The bleached layer at the outcrop shows similar features (increase in the density of deformation bands) compared to the bleached zones in the Cache Valley.

In addition, several minor faults (both synthetic and antithetic to the main fault) are located in the footwall of the main fault which were studied along a 60 m scanline (Figure 8(a)). Displacement measurements on the minor faults range from 44 cm to 2.47 m. The fault rocks observed in the fault cores include beige cataclasite, greenish-grey shale gouge, and sandstone lenses of different sizes in addition to calcite cementation (Figure 8(b)).

One of the antithetic normal faults is located close to the main fault (at 14 m distance from the main fault) and at 45.22 m above the base scanline (Figures 8(a) and 8(d)). The fault is trending ENE-WSW with a gentle dip of 31°SE. The fault core of the main fault is thicker and shows a larger variation in thickness compared to the cores of the minor faults (Figure 8(c)). Among the minor faults, the antithetic faults tend to be thicker than the synthetic faults in this locality (Figure 8(d)).

Table 1: A list of the scanlines and number of different types of faults in each scanline measured in Vallone di Santo Spirito. The following abbreviations were used: RF: reverse fault; NF: normal fault; RLSF: right-lateral strike-slip fault; LLSF: left-lateral strike-slip fault.

| Scanline number | Scanline length (m) | Number of faults | Fault type |
|---|---|---|---|
| 1 | 10 | 1 | RF (1) |
| 2 | 23 | 2 | Pretilted NF (2) |
| 3 | 123.5 | 9 | NF (6), RLSF (3) |
| 4 | 40 | 3 | RLSF (3) |
| 5 | 62 | 7 | NF (2), RF (4), RLSF (1) |
| 6 | 100 | 7 | RF (2), LLSF (5) |
| 7 | 40 | 2 | LLSF (2) |
| 8 | 30 | 1 | NF (1) |
| 9 | 62 | 4 | NF (3), RF (1) |
| 10 | 34 | 2 | NF (1), RF (1) |
| 11 | 50 | 4 | NF (1), RF (2), LLSF (1) |
| 12 | 33.3 | 3 | Pretilted NF (2), RLSF (1) |

*3.2. Faults in Carbonate Rocks.* This field locality is situated in the southern Apennines, eastern Italy, on the eastern edge of the Maiella Mountain, in Vallone di Santo Spirito (Figure 16). Measurements of fault core thickness and displacement were carried out on different fault types located in Vallone di Santo Spirito. A total of 12 scanlines, which include 45 faults and 693 fault core thickness, were measured in this outcrop (Table 1). Among these 45 faults, 18 are normal faults (4 of them are pretilted normal faults), 11 are reverse faults, and 16 are strike-slip faults, of which are 7 right-lateral and 9 left-lateral. The orientations of faults are as follows: pretilted normal faults NW-SE to E-W, dipping N; normal faults NE-SW, dipping SE; reverse faults NE-SW, dipping W; right-lateral strike-slip faults NE-SW to N-S, dipping W; and left-lateral strike-slip faults NW-SE, dipping S (Figure 17). The stratigraphic unit exposed in the study area is the carbonate platform unit of Morrone di Pacentro Formation of Early Cretaceous age [41], which is a massive, white micritic limestone. To the north of the studied locality, Cima delle Murelle limestone of the Late Cretaceous is exposed. Extensive weathering and erosion have resulted in a grey-brownish surface color related to secondary carbonate cementation in addition to many karsts and collapsed karst structures in the rocks observed throughout the study area. Pressure dissolution seams (PSS) are also observed parallel to the bedding, which in many cases have turned to parallel-bedding normal faulting and subsequent karsts.

The fault core includes a variety of fault rocks such as fault gouge, carbonate rock fragments, carbonate lenses, and breccia, which is sometimes cemented (Figure 9). Carbonate fault gouge (Figure 9(a)) was observed in the fault core of all the different fault types in the study area. The fault gouge could be uncemented and consists of very fine-grained beige-grey carbonate grains with carbonate fragments ranging in size from mm to dm (Figure 9(a)). Sometimes, the fault gouge is calcite cemented (Figure 9(c)). Fault breccia was observed in both cohesive (Figure 9(e)) and noncohesive forms (breccia pockets) in some of the fault cores, mainly in the fault core of the major strike-slip faults. In addition, small dissolution features are observed in the fault core (Figure 9(d)), which were excluded from the total fault core thickness at each level.

From 12 scanlines, only two examples of the scanlines (scanlines 3 and 5) with their associated faults and corresponding fault core measurements are presented in Figures 10 and 11. There are both normal faults parallel to bedding and strike-slip faults crossing the bedding in scanline 3 (Figure 10). Several large dissolution (karst) features are also observed along this scanline, which are usually located in the damage zone of the faults and stop by the fault core (Figure 10). These were not included in our measurements. Among faults presented in Figure 10, the right-lateral strike-slip faults have the thickest fault core. Scanline 5 in Figure 11 includes reverse faults in addition to normal and strike-slip faults. In Figure 11, the thicker fault cores belong to the right-lateral strike-slip and reverse faults.

*3.3. Comparison between Fault Core Thickness in Different Lithologies.* We have compiled our fault core thickness data for small faults of up to 10 m displacement in both siliciclastic and carbonate rocks and divided them in similar bins based on the maximum and minimum values of measurements in order to compare the distribution of the thickness data (Figure 12). In Figure 12, the majority of fault core thickness measurements fall within the 1 – 5 cm bin, which covers 38% of the siliciclastic data and 39% of the carbonate data. However, for fault cores in the range of 5 – 10 cm, carbonate rocks have a higher percentage (22%) in comparison to siliciclastic rocks (11%). This is also relevant to the 10 – 20 cm bin, in which carbonate rocks cover a higher percentage (18%) versus 10% in siliciclastic rocks. For larger bin sizes, the values drop for both siliciclastic and carbonate rocks. The largest fault core size categorized in the 250 – 2000 cm bin is only found in the siliciclastic rocks among our datasets (Figure 12).

The small faults (up to 5 m displacement) in both lithologies are also compared with respect to displacement data bins (Table 2). The average thickness values for similar displacement bins are in the same range and quite similar in both lithologies, only for $0.5 \leq D \leq 1$ m; the average thickness is slightly higher in carbonate rocks.

In order to study the scaling relationship between fault core thickness and displacement, we have correlated the average values of fault core thickness with the displacement of the corresponding fault for all the studied localities (Figure 13(a)). The thickness of fault lenses is excluded from the plot in Figure 13(a). The thickest fault cores in siliciclastic dataset come from the larger faults in the R-191 Canyon and Hidden Canyon localities (localities 1 and 2). Fault cores in these faults involve a more complex internal structure than smaller faults in other localities. Several slip surfaces, breccia, shale gouge, and rock fragments contribute to the thickness of the fault core in the R-191 Canyon locality. In the Hidden Canyon, several

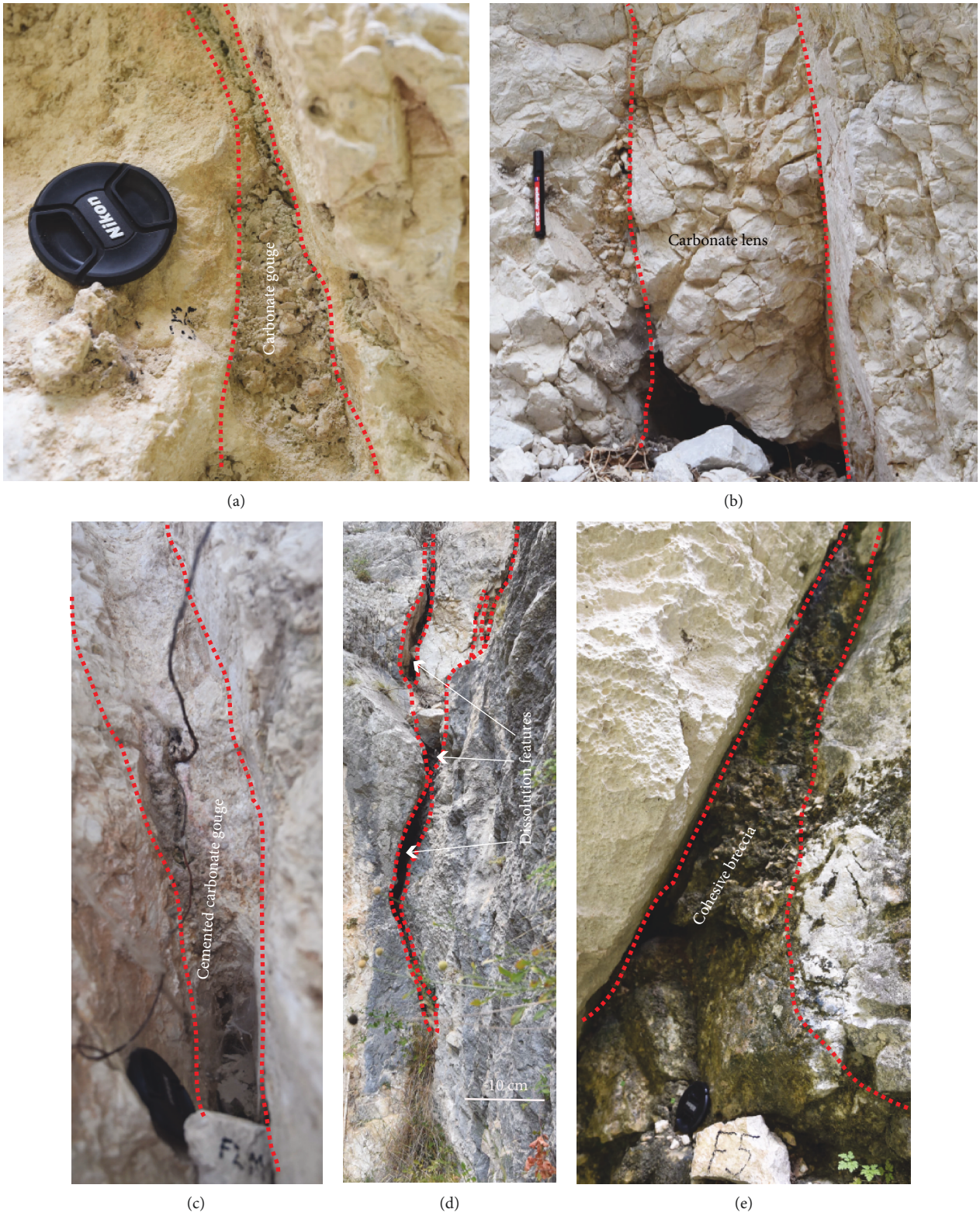


Figure 9: Different fault rocks observed in the studied fault cores in Vallone di Santo Spirito, Maiella. (a) Beige carbonate gouge observed in the fault core of a right-lateral strike-slip fault. Note the carbonate fragments that are incorporated in the gouge. (b) Carbonate lens trapped in the fault core of a right-lateral strike-slip fault. (c) White-brownish cemented fault gouge located in the fault core of a right-lateral strike-slip fault. (d) Dissolution features formed in dilation jogs along a strike-slip fault. (e) A cohesive breccia pocket observed in the fault core of a left-lateral strike-slip fault.

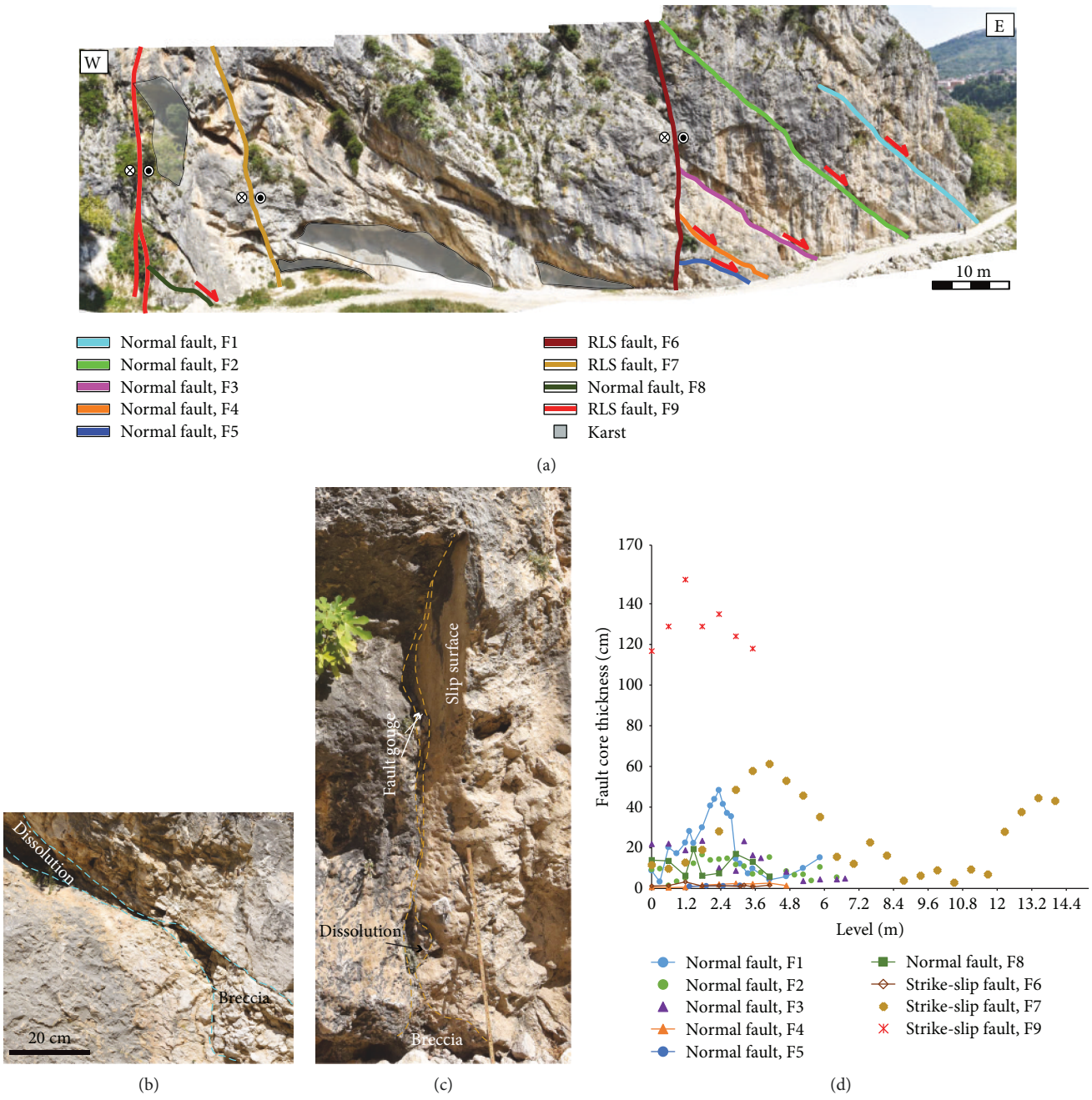


Figure 10: (a) Outcrop photo of the studied faults in scanline 3 in Vallone Santo Spirito (Maiella Mountain). The outcrop includes 6 normal and 3 strike-slip faults (right-lateral strike-slip (RLS)). (b) A closeup picture of the F1 internal core structure, indicating breccia and dissolution along the core. (c) A closeup picture of the F7 core, which shows breccia, dissolution features as well as fault gouge in the fault core. (d) Fault core thickness measurements performed both in the outcrop and on the photos along different heights of the faults.

fault gouges with different thickness are entrapped between slip surfaces, which have resulted in a thick fault core. The trend line fitted to the faulted carbonate rock data is a power law with an exponent close to one, which makes the relation almost linear. While for siliciclastic rocks, the exponent of the power law is lower (Figure 13(a)). When considering only faults with displacement less than 5 m in siliciclastic rocks in order to make a comparison with fault data in carbonates, the power law relation does not substantially change for these rocks (Figure 13(a)). From the power law relations, it is expected that for small faults with displacement less than 5 m, the fault core/displacement ($T/D$) ratio is relatively higher in carbonate rocks than siliciclastic rocks (Figure 13(a)). This could be related to the presence of breccia (Figure 9) in carbonate fault cores. The fault type might also have an effect on the fault core thickness in the studied carbonate rocks in Maiella, while in siliciclastic rocks, only normal faults have been considered.

Including fault lens thickness for faults in Utah localities in the plot presented in Figure 13(b) increases the $T/D$ ratio

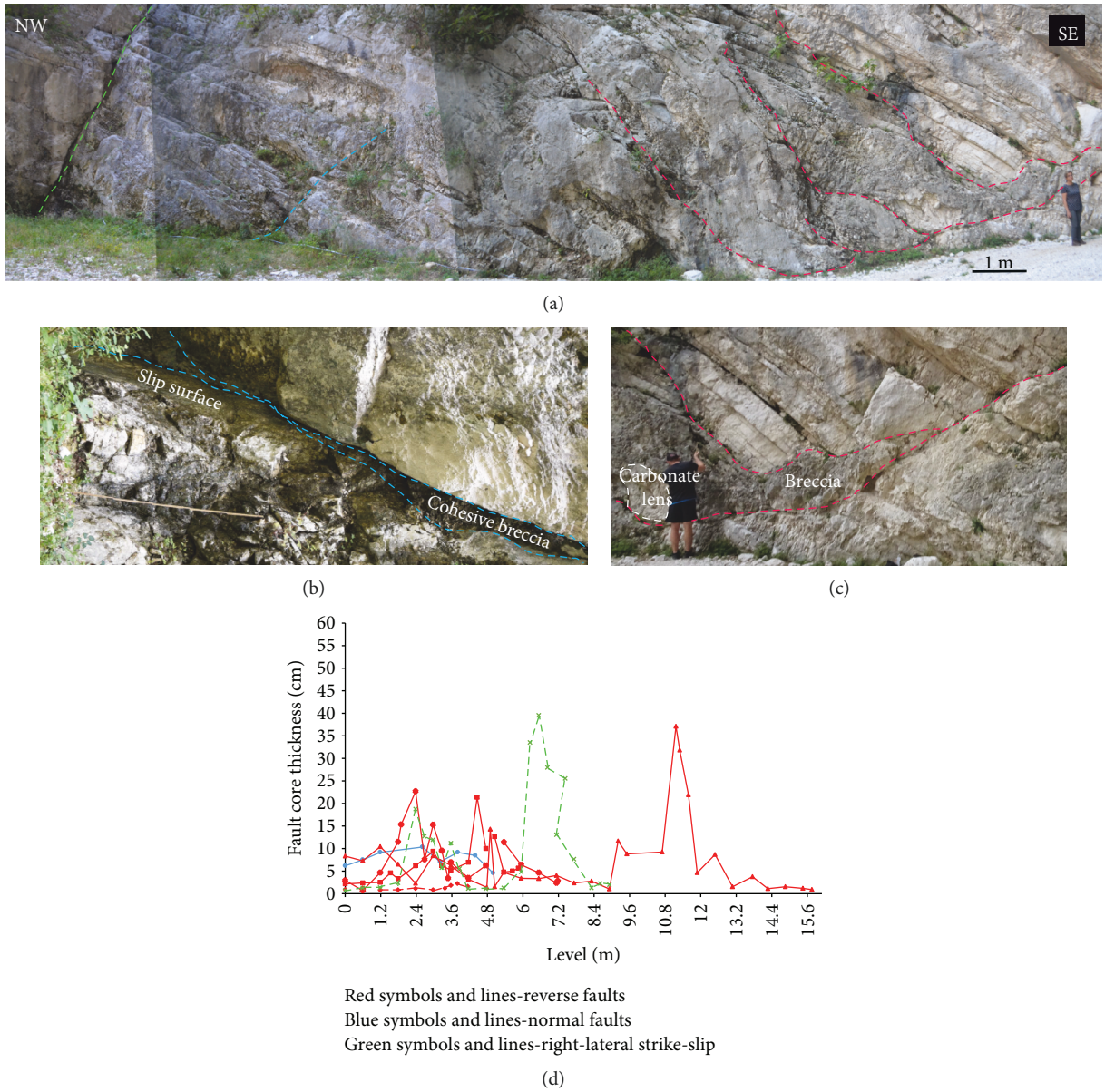


Figure 11: (a) Outcrop photo of faults measured in scanline 5 of the Vallone Santo Spirito (Maiella Mountain). There is a major reverse fault, which splays in several branches of reverse faults (shown in red dashed lines) in addition to a strike-slip fault and a normal fault. (b) A closeup picture of a pretilted normal fault in this locality. The image has been rotated 90 degrees for illustration purposes. (c) A closeup picture of the reverse fault core. (d) Fault core thickness measurements for the studied faults.

in comparison to the plot in Figure 13(a). Since there are a few data points for faults with 10 to 1000 m displacements in this plot (Figure 13(b)), fitting a curve to these data would not be statistically valid.

We have compared our datasets presented in Figure 13(a) with the published data, which includes datasets from siliciclastic, carbonate, and crystalline rocks (Figure 13(c) and Table 3). The range of datasets is comparable for all three types of lithologies. The figure shows that the relationship could vary based on lithology and three power laws could fit to the three datasets of siliciclastic, carbonate, and crystalline rocks (Figure 13(c) and Table 3). The power law fit to the carbonate rocks shows a smaller slope or exponent in comparison to the two other power law fits, although the coefficient of determination is lower for the power law fit to the carbonate rocks (Figure 13(c) and Table 3). This is in contrary to what we have observed in the first plot (Figure 13(c) and Table 3) and might be attributed to the fact that the published data may include fault core lenses that we have not included in our datasets. When comparing siliciclastic to crystalline rocks, the $T/D$ ratio is slightly higher in siliciclastic rocks than crystalline rocks with similar displacement values (Figure 13(c) and Table 3).

## 4. Discussion

This work provides a detailed study on fault cores of a variety of fault types by presenting fault core thickness data

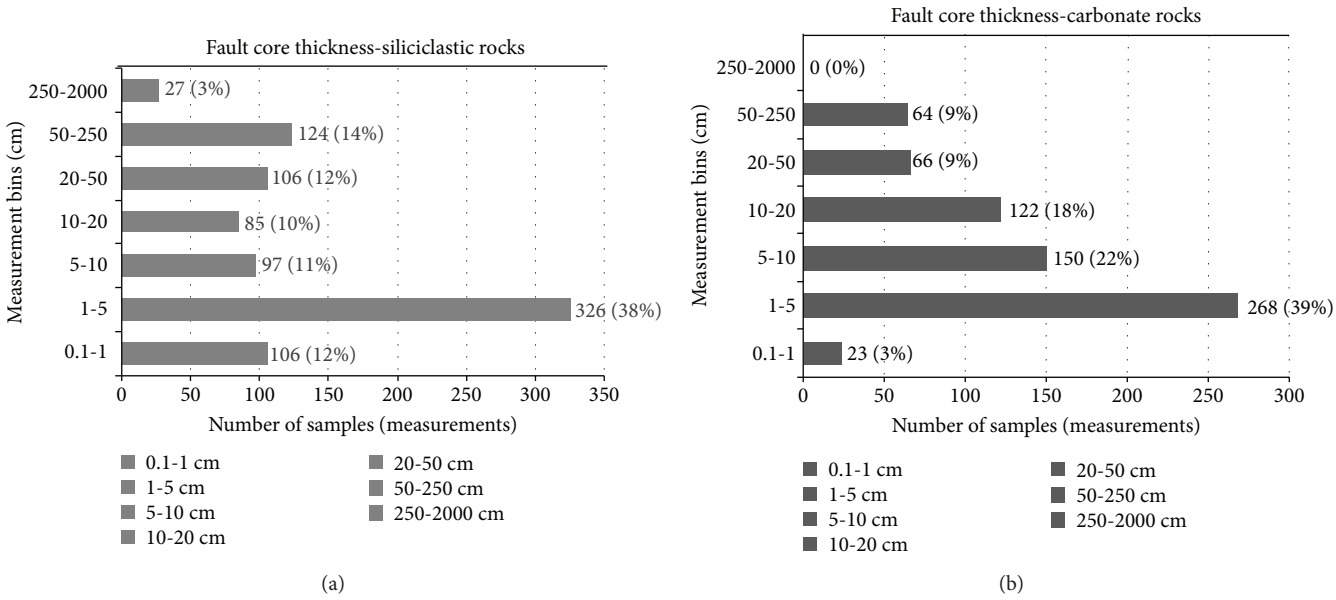


Figure 12: (a, b) Bar diagrams showing the number and percentage of fault core thickness distribution for small faults ($D < 10$ m) in siliciclastic and carbonate rocks, respectively.

Table 2: Displacement bins for faults in siliciclastic rocks and carbonate rocks. $D$ stands for displacement and $T$ for thickness.

| Displacement ($D$) | $D$ samples | Average $D$ (m) | Average $T$ (m) |
|---|---|---|---|
| *Siliciclastic rocks* | | | |
| <0.2 | 37 | 0.1 | 0.02 |
| 0.2-0.5 | 23 | 0.3 | 0.04 |
| 0.5-1 | 9 | 0.8 | 0.07 |
| 1-5 | 14 | 1.8 | 0.40 |
| *Carbonate rocks* | | | |
| <0.2 | 3 | 0.17 | 0.02 |
| 0.2-0.5 | 9 | 0.3 | 0.04 |
| 0.5-1 | 4 | 0.9 | 0.14 |
| 1-5 | 3 | 2.5 | 0.40 |

measurements along fault height and the relationship between the core thickness and displacement in siliciclastic and carbonate rocks. Several factors such as lithology, type of fault rocks, fault type and geometry, and displacement can affect the fault core internal structure and hence its thickness. In the following, some of these factors are discussed.

The presence of different fault rocks such as fault gouge, rock fragments, breccia, and lenses of host rock incorporated in the fault core tend to affect the internal core complexity and hence its thickness (e.g., [3, 6, 16, 42, 43]). This effect becomes significant where large lenses are included in the fault core. In this work, fault core lenses were measured in 53 small ($D < 10$ m) and large faults ($D > 10$ m). Some major fault core lenses influencing the fault core thickness were measured in segments of the Moab Fault in the Hidden Canyon, R-191 localities, and in two major right-lateral strike-slip faults located in Maiella. By including lenses in the data, there would be an increase by a factor ranging between 2 and 16 for the siliciclastic fault core thickness measurements and between 2 and 10 for the carbonate fault core thickness measurements. This factor is the ratio between the average core thickness including lenses to the average thickness excluding lenses. Bastesen and Braathen [16] suggested that fault core lenses become more common with increasing displacement and that the lens formation causes a great increase in core thickness and complexity.

The competency contrast between the faulted layers (mechanical stratigraphy) or between the rocks situated in the hanging wall and footwall has a substantial impact on the fault core thickness and complexity. In ANP locality, the presence of layers with different mechanical properties such as sandstone and shale has resulted in both localized and ductile deformations, respectively. This has led to variation in the fault core internal structure and thickness (Figures 14(a)–14(c)). Examples of different rock types in the hanging wall and footwall were observed in the Bartlett Fault (the Hidden Canyon) as well as the Cache Valley. In the Hidden Canyon, the Cedar Mountain Formation is situated in the hanging wall, while the Slick Rock and Moab Members of Entrada Sandstones are situated in the footwall. The Entrada Sandstone is a porous quartz sandstone and has less cement in comparison to the Cedar Mountain Formation, which is both calcite and quartz cemented [44]. This is also evident from the deformation features found in the damage zone of these rocks, which are mainly fractures (both shear fractures and joints) in the Cedar Mountain Formation and deformation bands in the Entrada Sandstone. Even comparing the two members of the Entrada Sandstone, the Moab Member is more porous and dominated by clusters of deformation bands. The lenses

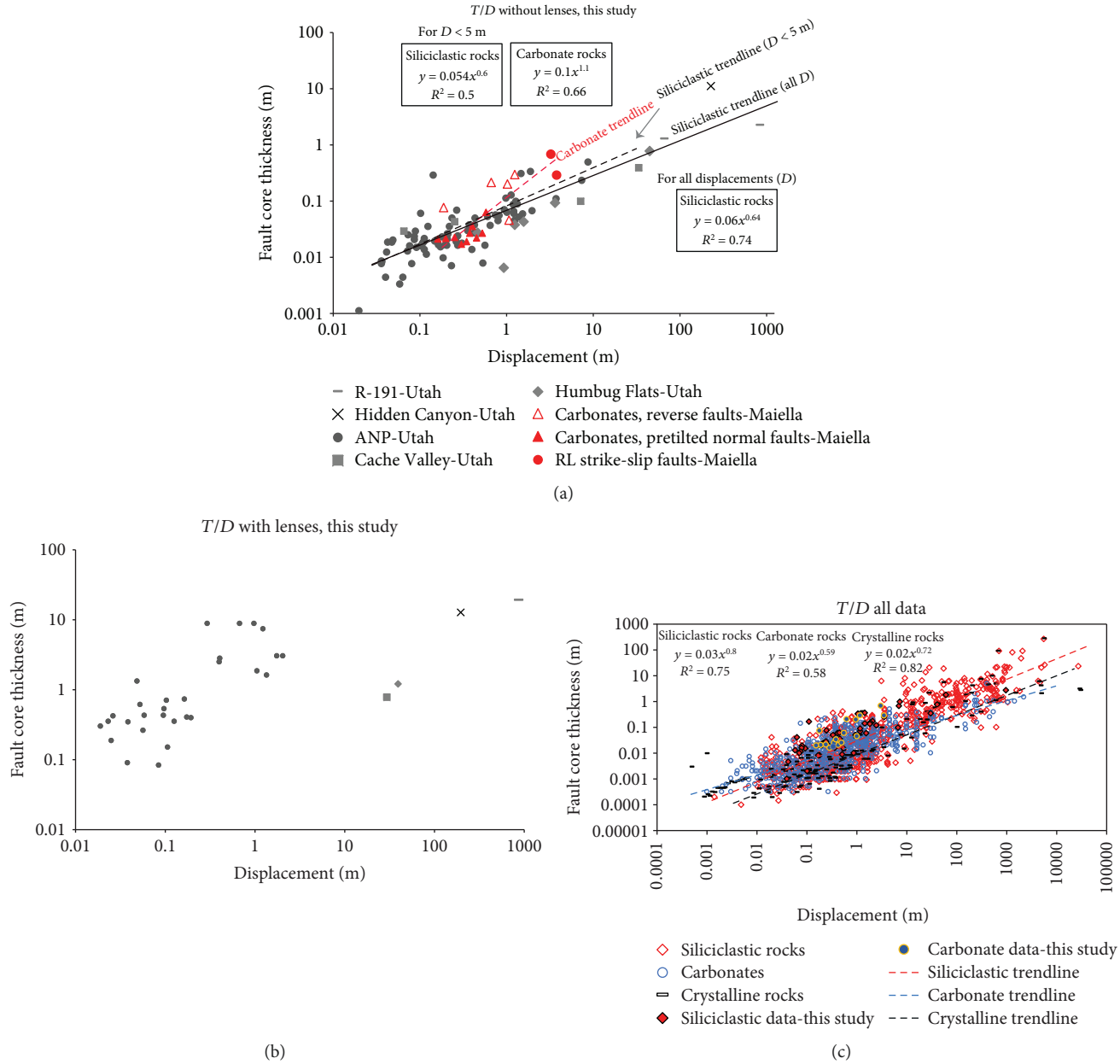


Figure 13: (a) Displacement-fault core thickness (without lens thickness) relation for some of the studied faults at different localities in this work. (b) Displacement-fault core thickness (with lens thickness) relation for some of the studied faults at different localities in Utah. (c) Displacement-fault core thickness relationship for a compiled database from published data and this study (without lens thickness). Note that three power laws fit to the data from faults in siliciclastic, carbonate, and crystalline rocks. The references used for this study are included in Table 3.

enveloped in the fault core are also from the Moab Member, which was the case for R-191 locality too. In the Cache Valley, the Navajo Sandstone in the footwall is more porous than the Slick Rock and Dewey Bridge Members. This is evident from the type and intensity of deformation features (deformation bands) in the Navajo Sandstone. In both the Cache Valley and Hidden Canyon, the porous sandstones include the bleaching path caused by reducing fluids circulating at some time in the rock. In the Cache Valley, the fault cores in the high-porosity bleached intervals were wider than the fault core in unbleached intervals.

Previous studies [29, 45] suggested that faults juxtaposing sandstone-shale have a thinner fault core in comparison to the faults juxtaposing sandstone-sandstone or shale-shale of similar displacement [30]. In contrary, in this study, we measured a significantly wider fault core in sandstone-shale-juxtaposed layers compared to sandstone-sandstone for similar displacement. This increase in core thickness could be related to smearing and drag of shaley layers into the fault core due to its ductile deformation (Figures 14(a)–14(c)).

The effect of lithology on fault geometry in normal faults juxtaposing heterogeneous sequences of siliciclastic rocks

Table 3: A list of the references used for the plot in Figure 13(c).

| Reference | Lithology |
|---|---|
| [7] | Siliciclastic rocks |
| [25] | Siliciclastic rocks |
| [30] | Siliciclastic rocks |
| [71] | Crystalline rocks |
| [22] | Siliciclastic rocks |
| [9] | Crystalline rocks |
| [72] | Siliciclastic rocks |
| [23] | Siliciclastic rocks |
| [3] | Siliciclastic rocks |
| [3] | Crystalline rocks |
| [11] | Siliciclastic rocks |
| [11] | Crystalline rocks |
| [16] | Carbonate rocks |
| [6] | Siliciclastic rocks |
| [6] | Carbonate rocks |

with competency contrasts (e.g., sandstone and shale) has been studied by several researchers ([23, 46, 47]). They found a steeper fault dip in competent layers such as limestone and sandstone and lower fault dip in less competent layers such as shale, which would result in fault refraction and possible dilation or relay zone along the fault [46]. Faults cutting through sandstone and shale layers might splay at asperities in less competent shale layers [23]. These fault splays, which are connected to the main slip surface, will continue to propagate and modify the dip contrast and eventually lead to breaching of the relay zone and incorporation of host rock lenses in the fault core [3] (Figures 14(a) and 14(b)).

In the R-191 Canyon locality in Utah, one large lens of the Moab Member is trapped between faults F1 and F2. In the Hidden Canyon, there are two significant fault lenses made out of the Moab Member. The presence of layers of different competencies and splays of the fault in the form of several slip surfaces might have contributed to the formation of the fault lenses in the Moab Fault [25]. The following hypothesis could explain the entrapment of these lenses. During fault propagation and modification of its architecture and geometry, the fault segments continue the breaching and breakdown of the relay zones formed between the fault splays, which traps the Moab Member. The remnant of the Moab Member relay ramp is enveloped in the lenses. This modification and breakdown of asperities could be continued until all the trapped fault rocks are comminuted and form a part of the fault gouge [3, 42, 43] (Figures 14(a) and 14(b)). Eventually, when all the lenses are crushed and become part of the fault gouge, it is expected that the $T/D$ ratio decreases in mature faults.

Bastesen et al. [6] investigated sequences of sandstone and shale layers as well as carbonates and shale layers and suggested that small faults with a displacement of less than 10 m have a relatively higher $T/D$ ratio in carbonates than faults with similar displacement in siliciclastic rocks. They also concluded that the fault core complexity and thickness do not change significantly when the displacement exceeds 10 m. Torabi and Berg [13] suggested that the slope of the power law relationship changes at a critical displacement (around 1 m displacement), with a higher slope for faults with less than 1 m displacement. This might be attributed to the more localization of strain with crushing most of the fault lenses into a fault gouge in larger mature faults that would result in a more localized fault core in comparison to the small faults. Our results (Figure 13(a)) support a fault model, in which the $T/D$ ratio could be relatively higher in small faults ($D \leq 5$ m) in carbonates compared to faults in siliciclastic rocks (e.g., [1, 6, 13]; Table 2); however, more data points of faults in carbonate rocks are needed to confirm this.

*4.1. Effect of Fault Core on Fluid Flow in Rocks.* Fault geometry and petrophysical properties are important parameters in reservoir modelling and fluid flow simulations of faulted rocks with applications toward petroleum production and exploration [1, 4, 30], hydrogeology (Bense et al., 2013), geothermal reservoirs [18], and $CO_2$ storage [17, 19]. The fault core is regarded as the key element for estimating the sealing and conductivity (transmissivity) potential of a fault zone, but great lateral variations in core thickness and type of fault rocks enveloped in the core increase the uncertainty of input parameters in the fault models. Different fault rocks in the fault core have different effects on the fault permeability. Fault gouge and shale smear have been reported to reduce cross fault permeability [48]. Whereas, host rock lenses incorporated in the fault core, which preserves the intact properties that could act as local conduits in an otherwise impermeable fault gouge [4, 6, 43]. In addition, the dissolution features and karsts located along faults in carbonate rocks of Maiella could provide pathways to the flow in such rocks if they are not filled with collapsed materials or cement at a later stage. The presence of uncemented breccia within the fault core could also contribute to the effective porosity and permeability and therefore across fault flow.

The datasets reported in this study provide a range of fault core thickness (variations along fault height) in different lithologies. These data can be used in the reservoir models to reduce the uncertainties in fault seal analysis. Excluding the thickness of permeable features such as lenses from the data leaves out the thickness of the low permeable part of the fault in our data. Handling the low permeable part of the fault is usually challenging for reservoir modelling since it could act as a barrier.

We envisage that the results of this study can contribute to the understanding of fault architecture and the interplay between fault displacement and core thickness ($D$-$T$ power law relationships), which reflects the fault growth process from small to large faults.

At present, few data are available from the petrophysical properties of the fault rocks within fault cores (e.g., [49]). A future study that combines similar geometric measurements of fault core and displacement with petrophysical properties

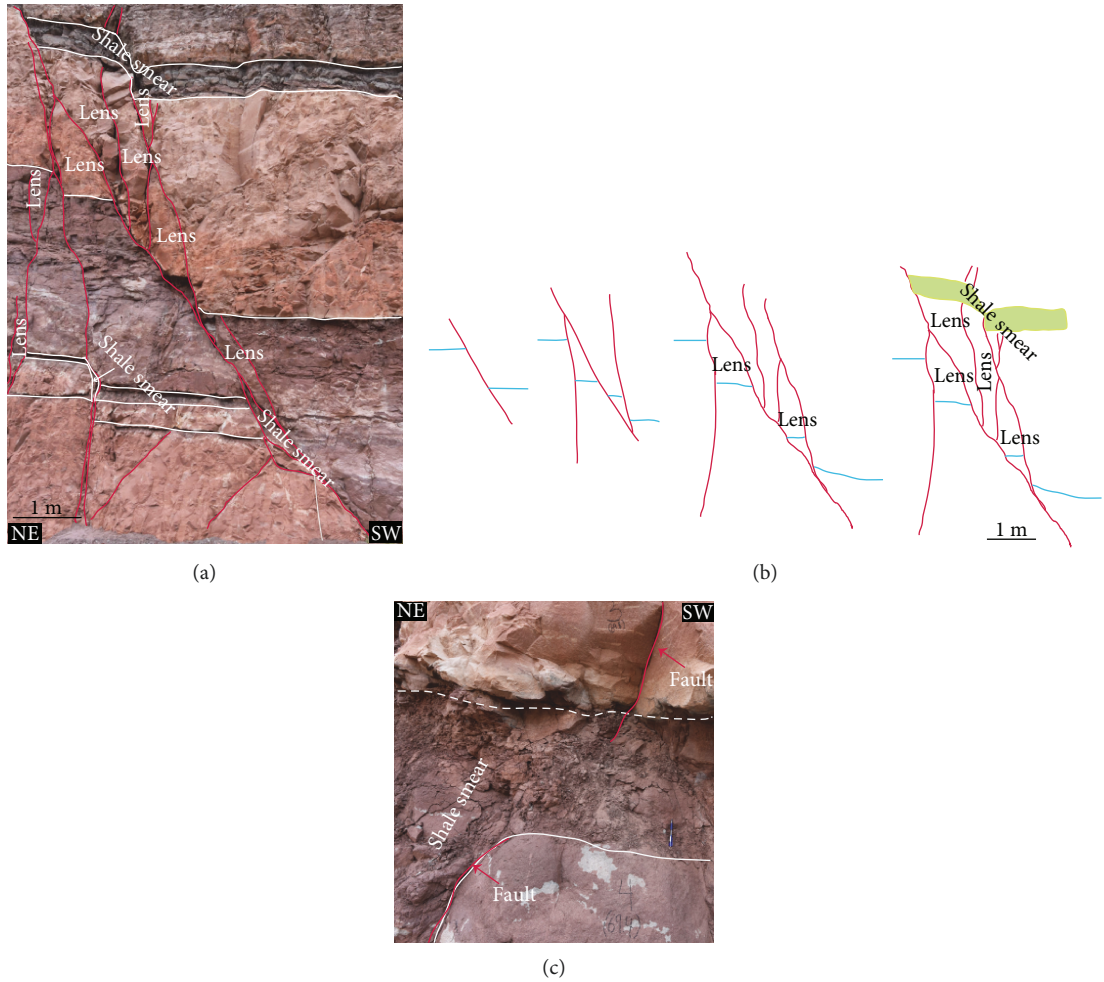


Figure 14: (a) A picture of the ANP outcrop that shows both fault core lenses trapped between relay zones and splays of the main fault, as well as the effect of mechanical stratigraphy on the fault core internal structure and geometry. (b) From left to right, a series of sketches showing a possible faulting process for the outcrop in (a). The fault grows in length and through linkage of the splays, which results in trapping fault lenses. The shale layer has smeared into the fault core as soon as the fault has cut through it at a later stage. (c) Effect of mechanical stratigraphy on fault core geometry and thickness. Note that in shaley layers, the fault core become thicker and its boundaries are diffuse, while in sandstone layers, the boundaries are sharper and the fault core is thinner, unless it entraps host rock lenses. Note that faults are illustrated in red lines and bedding in white lines.

of the corresponding fault rocks could certainly result in more accurate and realistic estimation of fault sealing and conductivity analysis of faulted rocks.

## 5. Conclusions

(i) The fault core internal structure and thickness are controlled by several factors, such as the fault geometry, displacement, interactions, and linkage between fault splays, fault rocks, lithology, and competency contrasts between faulted layers

(ii) The fault core thickness and complexity increase in the large faults in siliciclastic rocks with hundreds of meters of displacement because of the presence of shale gouge, breccia, and rock fragments entrapped between several slip surfaces

(iii) In general, small faults ($D \leq 5$ m) in carbonate and siliciclastic rocks show comparable $T/D$ ratio, with a slightly higher ratio in carbonate rocks

(iv) More accurate and realistic power law relationships between fault displacement and average core thickness are achieved by separating the data of different lithologies

## Appendix

### A. Geological Setting of Utah Field Localities in USA

Utah can be geologically divided into the western and eastern parts. The western part includes the Basin and Range Province, which was affected by considerable crustal thinning and extension. The eastern part includes the Utah branches

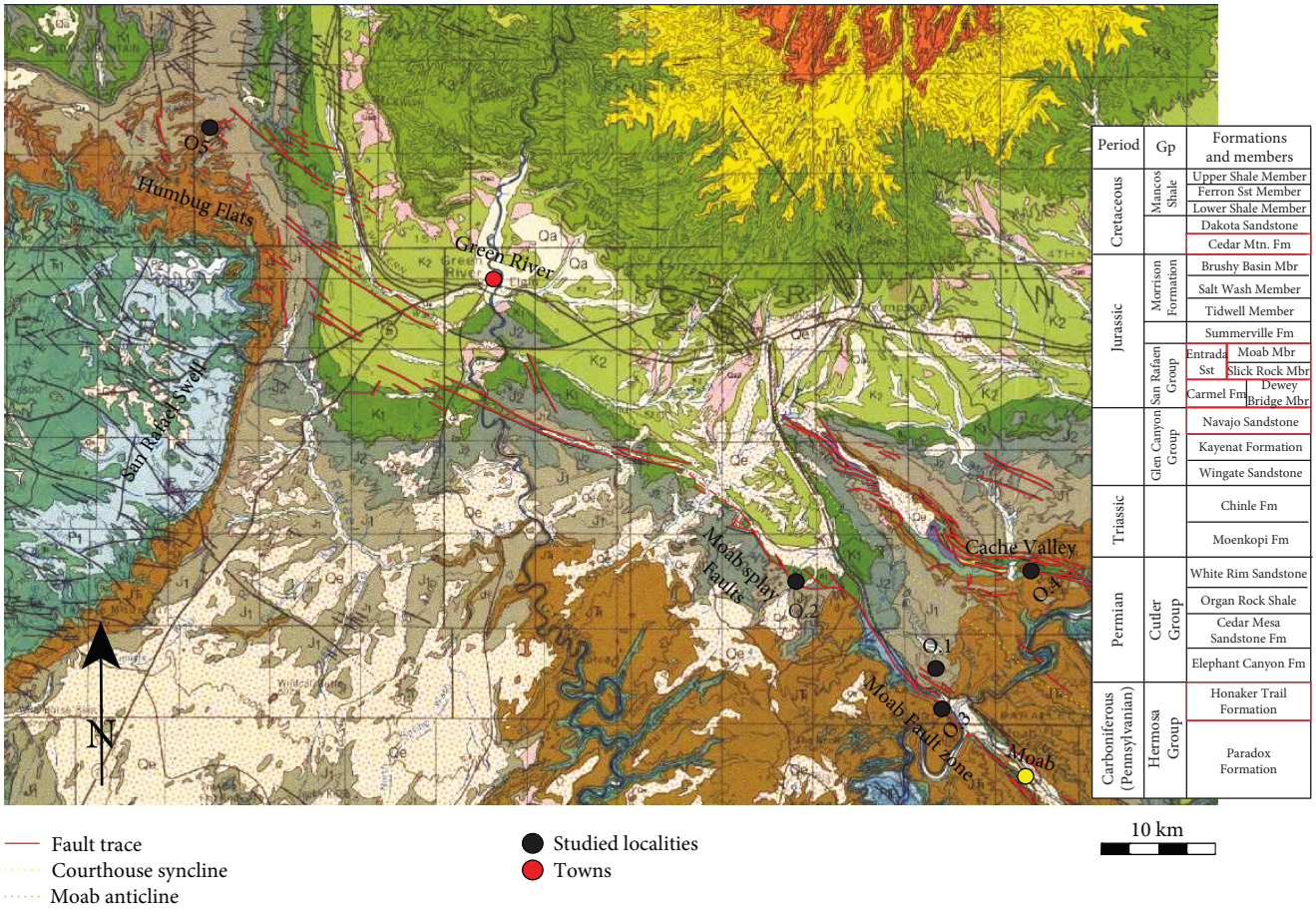


FIGURE 15: Geological map of Utah together with the stratigraphic column highlighting the studied formations. Note that the studied outcrops (O#) have been identified on the map. Modified after the geological map by Doelling [69].

of the Rocky Mountains to the North [50] and the Colorado Plateau provinces to the south. The Colorado Plateau provinces are relatively unaffected by the extension and have been elevated relative to the Basin and Range Province [51]. However, some deformation within the Colorado Plateau has occurred, such as intrusion of igneous laccoliths into the sedimentary succession in southeastern Utah, uplifts across the Plateau, e.g., San Rafael Swell and the Uncompahgre Ridge [52, 53]. Different basins have also been formed due to buckling and subsidence on the plateau, such as the Paradox and the Uinta Basins [33, 54].

The Paradox Basin is a large northwest-trending sedimentary foreland basin, which developed along the reactivated Precambrian basement faults along the southwestern flank of the Uncompahgre Ridge [52, 54]. Rapid subsidence of the basin and repeated sea level changes, combined with high evaporation rates, led to the formation of the Paradox Formation during the Middle Pennsylvanian. This resulted in accumulation of approximately 3 km thick dolomites, black organic shales, and evaporates [52, 54]. During the Permian, high depositional rates of sediments into the basin led to subsidence. With increasing the weight of accumulated sediments over the ductile evaporates in the Paradox Formation, the salt started to flow or be migrated, creating the salt-cored anticlines in the Paradox Basin. These salt-cored anticlines led to later deformation of the northern part of the Paradox Basin, creating the Paradox fault-and-fold belt, and the major Moab Fault zone [33, 54]. Four of the five localities studied in Utah are located in the Paradox Basin including the ANP, R-191 Canyon, Hidden Canyon, and Cache Valley, Figure 15.

Three of these localities (ANP, R-191, and Hidden Canyon) are collected along the Moab Fault zone, which is a 45 km long normal fault zone located above the Paradox Basin. The fault trace extends north-westwards from the Moab-Spanish Valley salt anticline along the southwestern flank of the Courthouse syncline [33]. The fault offsets an approximately 5000 m thick sedimentary sequence spanning from the Pennsylvanian to Cretaceous with a maximum surface dip-slip displacement of ~960 m [14, 25, 55] at the surface, but the displacement increases to 1800 m in the subsurface [25]. The main activities of the Moab Fault zone occurred during Triassic-Middle Jurassic associated with salt migration and from Late Cretaceous-Early Paleogene related to Laramide orogeny (Foxford et al. [33]. However, there are several controversial deformation mechanisms for the Moab Fault zone in the literature: (i) Mesozoic-Cenozoic extension that initiated the salt migration [25, 55, 56], (ii) subsidence as

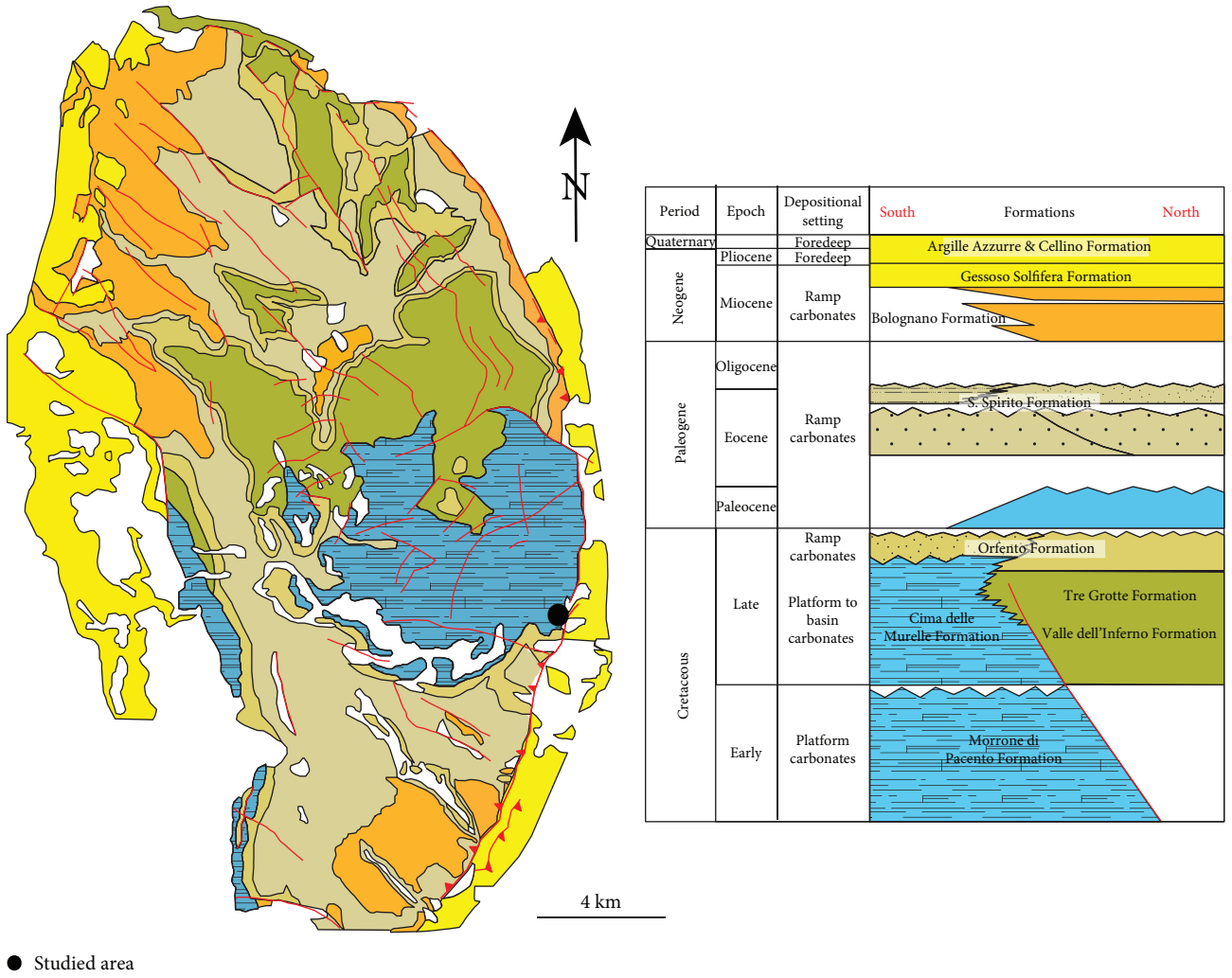


FIGURE 16: Geological map of Maiella with the geological units from Cretaceous until the present (modified from Di Cuia et al. [61], Aydin et al. [65], and Masini et al. [68]).

a result of salt dissolution and collapse [14, 54], (iii) tertiary extension and reactivation of basement faults due to a relaxation stage of the Laramide orogeny [24, 33], and (iv) Late Tertiary thin-skinned extension [57].

The Humbug Flats (the fifth studied locality in Utah) locality is situated on the northern edge of the San Rafael Swell outside the Paradox Basin (Figure 15). The studied normal faults are suggested to have developed due to the uplift of the major, dome-shaped, asymmetric anticline of the San Rafael Swell, during the Laramide orogeny [22, 58–60].

## B. Geological Setting of Maiella Field Localities in Italy

The Maiella Mountain formed during the central Apenninic fold-and-thrust belt, which is one of several interconnected Mediterranean orogeny that developed under the Late Cretaceous-Early Cenozoic closure of the Tethys Ocean [41]. The formation of the Apenninic fold-and-thrust belt incorporated different carbonate platform systems and allochthonous units onto the Italian mainland, forming the Southern Apennines. One of these carbonate platforms was the Apulian Platform, where the Maiella Mountain is presently situated (Figure 16; [61–64]). The main thrusting and folding activity occurred during Oligocene-Pliocene, when the Maiella anticline formed [63, 65–67]. The Maiella Mountain includes the easternmost major thrust sheet within the Apenninic fold-and-thrust belt [65].

The Maiella anticline is an approximately 30 km long, 10-15 km wide asymmetric anticline, with a steeply dipping eastern forelimb bounded by a basal thrust fault [63, 66, 68]. The study area is located on the eastern forelimb of Maiella Mountain in Vallone di Santo Spirito, where a complex fault and fracture network is exposed (Figure 16). The faulting within the Maiella anticline consists of normal and strike-slip faults and some reverse faults. These structures reflect four main tectonic events including the following: ENE-WSW extensional syn-rifting in the Tethys Ocean until Late Cretaceous resulting in tilting preexisting normal faults; extension phase in the Late Miocene resulting in normal

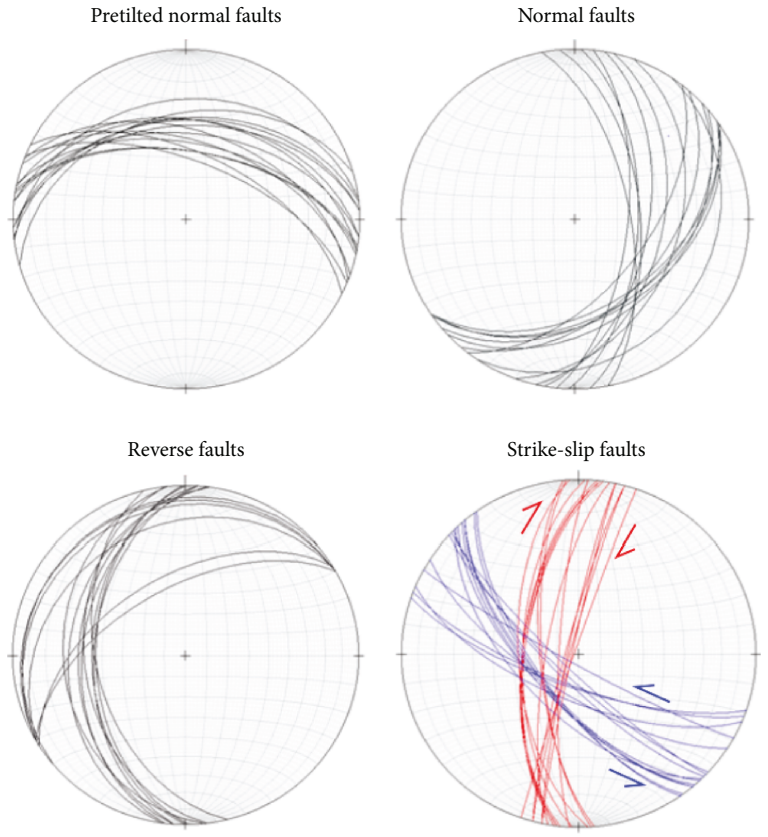


Figure 17: Stereoplots of fault orientations in Vallone di Santo Spirito, Maiella Mountain.

faults; E-W-oriented thrusting and folding during the Apenninic fold-and-thrust belt which formed reverse faults; and finally strike-slip faulting during Pleistocene responsible for strike-slip faults [61] (Figure 17).

## Data Availability

The data have been provided in different tables and plots (figures) in the manuscript.

## Conflicts of Interest

The authors declare that they have no conflicts of interest.

## Acknowledgments

This work was supported by the Norwegian Research Council through the NORRUSS and Petromaks2 Programs under Project 243628. Thanks are due to the authorities of the Maiella National Park for the permission to conduct the field work.

## References

[1] A. Braathen, J. Tveranger, H. Fossen et al., "Fault facies and its application to sandstone reservoirs," *AAPG Bulletin*, vol. 93, no. 7, pp. 891–917, 2009.

[2] J. S. Caine, J. P. Evans, and C. B. Forster, "Fault zone architecture and permeability structure," *Geology*, vol. 24, no. 11, pp. 1025–1028, 1996.

[3] C. Childs, T. Manzocchi, J. J. Walsh, C. G. Bonson, A. Nicol, and M. P. J. Schöpfer, "A geometric model of fault zone and fault rock thickness variations," *Journal of Structural Geology*, vol. 31, no. 2, pp. 117–127, 2009.

[4] N. Fredman, J. Tveranger, S. Semshaug, A. Braathen, and E. Sverdrup, "Sensitivity of fluid flow to fault core architecture and petrophysical properties of fault rocks in siliciclastic reservoirs: a synthetic fault model study," *Petroleum Geoscience*, vol. 13, no. 4, pp. 305–320, 2007.

[5] R. J. Knipe, G. Jones, and Q. J. Fisher, "Faulting, fault sealing and fluid flow in hydrocarbon reservoirs: an introduction," *Geological Society, London, Special Publications*, vol. 147, no. 1, pp. vii–xxi, 1998.

[6] E. Bastesen, A. Braathen, and T. Skar, "Comparison of scaling relationships of extensional fault cores in tight carbonate and porous sandstone reservoirs," *Petroleum Geoscience*, vol. 19, no. 4, pp. 385–398, 2013.

[7] J. P. Evans, "Thickness-displacement relationships for fault zones," *Journal of Structural Geology*, vol. 12, no. 8, pp. 1061–1065, 1990.

[8] H. Fossen and A. Rotevatn, "Fault linkage and relay structures in extensional settings—a review," *Earth-Science Reviews*, vol. 154, pp. 14–28, 2016.

[9] Z. K. Shipton, A. M. Soden, J. D. Kirkpatrick, A. M. Bright, and R. J. Lunn, "How thick is a fault? Fault displacement-thickness scaling revisited," in *Earthquakes: Radiated energy and the*

*physics of faulting*, vol. 170 of Geophysical Monograph Series, , pp. 193–198, AGU (American Geological Union), 2006.

[10] J. J. Walsh and J. Watterson, "Analysis of the relationship between displacements and dimensions of faults," *Journal of Structural Geology*, vol. 10, no. 3, pp. 239–247, 1988.

[11] C. A. J. Wibberley, G. Yielding, and G. di Toro, "Recent advances in the understanding of fault zone internal structure: a review," *Geological Society, London, Special Publications*, vol. 299, no. 1, pp. 5–33, 2008.

[12] R. A. Schultz and H. Fossen, "Terminology for structural discontinuities," *AAPG Bulletin*, vol. 92, no. 7, pp. 853–867, 2008.

[13] A. Torabi and S. S. Berg, "Scaling of fault attributes: a review," *Marine and Petroleum Geology*, vol. 28, no. 8, pp. 1444–1460, 2011.

[14] S. S. Berg and T. Skar, "Controls on damage zone asymmetry of a normal fault zone: outcrop analyses of a segment of the Moab fault, SE Utah," *Journal of Structural Geology*, vol. 27, no. 10, pp. 1803–1822, 2005.

[15] A. Billi, F. Salvini, and F. Storti, "The damage zone-fault core transition in carbonate rocks: implications for fault growth, structure and permeability," *Journal of Structural Geology*, vol. 25, no. 11, pp. 1779–1794, 2003.

[16] E. Bastesen and A. Braathen, "Extensional faults in fine grained carbonates – analysis of fault core lithology and thickness–displacement relationships," *Journal of Structural Geology*, vol. 32, no. 11, pp. 1609–1628, 2010.

[17] F. Cappa and J. Rutqvist, "Modeling of coupled deformation and permeability evolution during fault reactivation induced by deep underground injection of $CO_2$," *International Journal of Greenhouse Gas Control*, vol. 5, no. 2, pp. 336–346, 2011.

[18] S. Loveless, M. Pluymaekers, D. Lagrou, E. De Boever, H. Doornenbal, and B. Laenen, "Mapping the geothermal potential of fault zones in the Belgium-Netherlands border region," *Energy Procedia*, vol. 59, pp. 351–358, 2014.

[19] J. Rohmer, T. K. Nguyen, and A. Torabi, "Off-fault shear failure potential enhanced by high-stiff/low-permeable damage zone during fluid injection in porous reservoirs," *Geophysical Journal International*, vol. 202, no. 3, pp. 1566–1580, 2015.

[20] A. Torabi, R. H. Gabrielsen, H. Fossen et al., "Strain localization in sandstone and its implications for CO2 storage," *First Break*, vol. 33, no. 7, pp. 81–92, 2015.

[21] B. Alaei and A. Torabi, "Seismic imaging of fault damaged zone and its scaling relation with displacement," *Interpretation*, vol. 5, no. 4, pp. SP83–SP93, 2017.

[22] Z. Shipton, J. Evans, and L. Thompson, "The geometry and thickness of deformation-band fault core and its influence on sealing characteristics of deformation-band fault zones," *AAPG Memoir*, vol. 85, pp. 181–195, 2005.

[23] W. van der Zee, C. A. J. Wibberley, and J. L. Urai, "The influence of layering and pre-existing joints on the development of internal structure in normal fault zones: the Lodève basin, France," *Geological Society, London, Special Publications*, vol. 299, no. 1, pp. 57–74, 2008.

[24] N. C. Davatzes, P. Eichhubl, and A. Aydin, "Structural evolution of fault zones in sandstone by multiple deformation mechanisms: Moab Fault, southeast Utah," *Geological Society of America Bulletin*, vol. 117, no. 1, pp. 135–148, 2005.

[25] K. A. Foxford, J. J. Walsh, J. Watterson, I. R. Garden, S. C. Guscott, and S. D. Burley, "Structure and content of the Moab Fault zone, Utah, USA, and its implications for fault seal prediction," *Geological Society, London, Special Publications*, vol. 147, no. 1, pp. 87–103, 1998.

[26] S. D. Knott, "Fault zone thickness versus displacement in the Permo-Triassic sandstones of NW England," *Journal of the Geological Society*, vol. 151, no. 1, pp. 17–25, 1994.

[27] J. G. Solum and B. A. H. Huisman, "Toward the creation of models to predict static and dynamic fault-seal potential in carbonates," *Petroleum Geoscience*, vol. 23, no. 1, pp. 70–91, 2017.

[28] E. Robertson, "Relationship of fault displacement to gouge and breccia thickness," *Mining Engineering*, vol. 35, pp. 1426–1432, 1983.

[29] S. D. Knott, A. Beach, P. J. Brockbank, J. Lawson Brown, J. E. McCallum, and A. I. Welbon, "Spatial and mechanical controls on normal fault populations," *Journal of Structural Geology*, vol. 18, no. 2-3, pp. 359–372, 1996.

[30] S. Sperrevik, P. A. Gillespie, Q. J. Fisher, T. Halvorsen, and R. J. Knipe, "Empirical estimation of fault rock properties," in *Hydrocarbon Seal Quantification, Norwegian Petroleum Society Conference*, vol. 11 of Norwegian Petroleum Society Special Publications, , pp. 109–125, Norwegian Petroleum Society, 2002.

[31] D. Kolyukhin and A. Torabi, "Statistical analysis of the relationships between faults attributes," *Journal of Geophysical Research: Solid Earth*, vol. 117, no. B5, 2012.

[32] D. T. Seifried, "Faults architecture and their scaling relationships: insights into fault core thickness and fault displacement: MSc. Thesis," University of Bergen, 2012.

[33] K. Foxford, I. Garden, S. Guscott et al., "The field geology of the Moab Fault: geology and resources of the Paradox Basin," *Utah Geological Association Publication*, vol. 25, pp. 265–283, 1996.

[34] T. E. S. Johansen and H. Fossen, "Internal geometry of fault damage zones in interbedded siliciclastic sediments," *Geological Society, London, Special Publications*, vol. 299, no. 1, pp. 35–56, 2008.

[35] M. A. Chan, W. T. Parry, and J. R. Bowman, "Diagenetic hematite and manganese oxides and fault-related fluid flow in Jurassic sandstones, southeastern Utah," *AAPG Bulletin*, vol. 84, no. 9, pp. 1281–1310, 2000.

[36] V. F. Nuccio and S. M. Condon, *Burial and Thermal History of the Paradox Basin, Utah and Colorado, and Petroleum Potential of the Middle Pennsylvanian Paradox Formation*, U.S. Geological Survey Bulletin 2000-O, 1996.

[37] R. Alikarami, A. Torabi, D. Kolyukhin, and E. Skurtveit, "Geostatistical relationships between mechanical and petrophysical properties of deformed sandstone," *International Journal of Rock Mechanics and Mining Sciences*, vol. 63, pp. 27–38, 2013.

[38] N. C. Davatzes and A. Aydin, "Overprinting faulting mechanisms in high porosity sandstones of SE Utah," *Journal of Structural Geology*, vol. 25, no. 11, pp. 1795–1813, 2003.

[39] H. H. Doelling, "Geology of Salt Valley anticline and Arches National Park, Grand County, Utah," in *Salt Deformation in the Paradox Region*, H. H. Doelling, C. G. Oviatt, and P. W. Huntoon, Eds., p. 58, Utah Geological and Mineral Survey, Salt Lake City UT, 1988.

[40] A. Braathen, K. Ogata, E. Bastesen, and R. Gabrielsen, "Fractures and structural elements of extensional faults; importance for seal bypass systems in sandstone reservoir successions," in *Proceedings Proceedings of the 3rd International Conference on*

*Fault and Top Seals—From Characterization to Modelling*, Montepellier, France, 2012.

[41] A. Festa, C. Accotto, F. Coscarelli, E. Malerba, and G. Palazzin, "Geology of the Aventino River Valley (eastern Majella, Central Italy)," *Journal of Maps*, vol. 10, no. 4, pp. 584–599, 2014.

[42] R. H. Gabrielsen, A. Braathen, M. Kjemperud, and M. L. R. Valdresbråten, "The geometry and dimensions of fault-core lenses," *Geological Society, London, Special Publications*, vol. 439, no. 1, pp. 249–269, 2017.

[43] M. Lindanger, R. H. Gabrielsen, and A. Braathen, "Analysis of rock lenses in extensional faults," *Norwegian Journal of Geology*, vol. 87, pp. 361–372, 2007.

[44] E. Ellingsen, "Interaction of diagenesis and deformation of faulted sandstone reservoirs: master of science thesis in petroleum geology," Department of Earth Science, University Of Bergen, 2011.

[45] H. Fossen and J. Hesthammer, "Possible absence of small faults in the Gullfaks field, northern North Sea: implications for downscaling of faults in some porous sandstones," *Journal of Structural Geology*, vol. 22, no. 7, pp. 851–863, 2000.

[46] D. A. Ferrill, A. P. Morris, R. N. McGinnis, K. J. Smart, S. S. Wigginton, and N. J. Hill, "Mechanical stratigraphy and normal faulting," *Journal of Structural Geology*, vol. 94, pp. 275–302, 2017.

[47] D. C. P. Peacock and D. J. Sanderson, "Effects of layering and anisotropy on fault geometry," *Journal of the Geological Society*, vol. 149, no. 5, pp. 793–802, 1992.

[48] R. B. Færseth, E. Johnsen, and S. Sperrevik, "Methodology for risking fault seal capacity: implications of fault zone architecture," *AAPG Bulletin*, vol. 91, no. 9, pp. 1231–1246, 2007.

[49] A. Torabi, H. Fossen, and A. Braathen, "Insight into petrophysical properties of deformed sandstone reservoirs," *AAPG Bulletin*, vol. 97, no. 4, pp. 619–637, 2013.

[50] L. Hintze and B. Kowallis, "Geologic history of Utah: Brigham Young University Geology Studies special publication 9, Tech. rept," Brigham Young University, Salt Lake City, UT, 2009.

[51] J. L. Pederson, R. D. Mackley, and J. L. Eddleman, "Colorado plateau uplift and erosion evaluated using GIS," *GSA Today*, vol. 12, no. 8, pp. 4–10, 2002.

[52] D. L. Barbeau, "A flexural model for the Paradox Basin: implications for the tectonics of the Ancestral Rocky Mountains," *Basin Research*, vol. 15, no. 1, pp. 97–115, 2003.

[53] A. P. Bump and G. H. Davis, "Late Cretaceous–Early Tertiary Laramide deformation of the northern Colorado Plateau, Utah and Colorado," *Journal of Structural Geology*, vol. 25, no. 3, pp. 421–440, 2003.

[54] B. D. Trudgill, "Evolution of salt structures in the northern Paradox Basin: controls on evaporite deposition, salt wall growth and supra-salt stratigraphic architecture," *Basin Research*, vol. 23, no. 2, pp. 208–238, 2011.

[55] T. E. S. Johansen, H. Fossen, and R. Kluge, "The impact of syn-faulting porosity reduction on damage zone architecture in porous sandstone: an outcrop example from the Moab Fault, Utah," *Journal of Structural Geology*, vol. 27, no. 8, pp. 1469–1485, 2005.

[56] J. G. Solum, N. C. Davatzes, and D. A. Lockner, "Fault-related clay authigenesis along the Moab Fault: implications for calculations of fault rock composition and mechanical and hydrologic fault zone properties," *Journal of Structural Geology*, vol. 32, no. 12, pp. 1899–1911, 2010.

[57] S. S. Olig, C. H. Fenton, J. McCleary, and I. G. Wong, "The earthquake potential of the Moab Fault and its relation to salt tectonics in the Paradox Basin, Utah," *Geology and Resources of the Paradox Basin Utah Geological Association Guidebook*, A. C. Huffman Jr., W. R. Lund, and L. H. Godwin, Eds., vol. 25, pp. 246–251, USGS (US Geological Survey),Utah department of natural resources, 1996.

[58] N. C. Davatzes, A. Aydin, and P. Eichhubl, "Overprinting faulting mechanisms during the development of multiple fault sets in sandstone, Chimney Rock fault array, Utah, USA," *Tectonophysics*, vol. 363, no. 1-2, pp. 1–18, 2003.

[59] J. M. English and S. T. Johnston, "The Laramide orogeny: what were the driving forces?," *International Geology Review*, vol. 46, no. 9, pp. 833–838, 2004.

[60] K. Ogata, K. Senger, A. Braathen, and J. Tveranger, "Fracture corridors as seal-bypass systems in siliciclastic reservoir-cap rock successions: field-based insights from the Jurassic Entrada Formation (SE Utah, USA)," *Journal of Structural Geology*, vol. 66, pp. 162–187, 2014.

[61] R. Di Cuia, A. Shakerley, M. Masini, and D. Casabianca, "Integrating outcrop data at different scales to describe fractured carbonate reservoirs: example of the Maiella carbonates, Italy," *First Break*, vol. 27, no. 3, pp. 45–55, 2009.

[62] E. Di Luzio, M. Saroli, C. Esposito, G. Bianchi-Fasani, G. P. Cavinato, and G. Scarascia-Mugnozza, "Influence of structural framework on mountain slope deformation in the Maiella anticline (Central Apennines, Italy)," *Geomorphology*, vol. 60, no. 3-4, pp. 417–432, 2004.

[63] G. P. Eberli, D. Bernoulli, D. Sanders, and A. Vecsei, "From aggradation to progradation: the Maiella platform, Abruzzi, Italy," *Atlas of Cretaceous Carbonate Platforms: AAPG Memoir*, T. Simo, R. W. Scott, and J. P. Masse, Eds., pp. 213–232, AAPG(American Association of Petrolum Geologist), 1993.

[64] M. Santantonio, D. Scrocca, and L. Lipparini, "The Ombrina-Rospo Plateau (Apulian Platform): evolution of a carbonate platform and its margins during the Jurassic and Cretaceous," *Marine and Petroleum Geology*, vol. 42, pp. 4–29, 2013.

[65] A. Aydin, M. Antonellini, E. Tondi, and F. Agosta, "Deformation along the leading edge of the Maiella thrust sheet in Central Italy," *Journal of Structural Geology*, vol. 32, no. 9, pp. 1291–1304, 2010.

[66] B. Graham, M. Antonellini, and A. Aydin, "Formation and growth of normal faults in carbonates within a compressive environment," *Geology*, vol. 31, no. 1, pp. 11–14, 2003.

[67] V. Scisciani, E. Tavarnelli, and F. Calamita, "The interaction of extensional and contractional deformations in the outer zones of the Central Apennines, Italy," *Journal of Structural Geology*, vol. 24, no. 10, pp. 1647–1658, 2002.

[68] M. Masini, S. Bigi, J. Poblet, M. Bulnes, R. D. Cuia, and D. Casabianca, "Kinematic evolution and strain simulation, based on cross-section restoration, of the Maiella Mountain: an analogue for oil fields in the Apennines (Italy)," *Geological Society, London, Special Publications*, vol. 349, no. 1, pp. 25–44, 2011.

[69] H. Doelling, "Geologic map of the Moab 30'x 60'quadrangle: Grand County, Utah," *Utah Geological Survey Map*, vol. 180, no. 3, 2001.

[70] M. U. Johannessen, *Fault Core and Its Geostatistical Analysis: Insight into the Fault Core Thickness and Fault Displacement*, The University Of Bergen, 2017.

[71] G. Di Toro and G. Pennacchioni, "Fault plane processes and mesoscopic structure of a strong-type seismogenic fault in tonalites (Adamello batholith, Southern Alps)," *Tectonophysics*, vol. 402, no. 1-4, pp. 55–80, 2005.

[72] W. van der Zee and J. L. Urai, "Processes of normal fault evolution in a siliciclastic sequence: a case study from Miri, Sarawak, Malaysia," *Journal of Structural Geology*, vol. 27, no. 12, pp. 2281–2300, 2005.